Gondwana Research 22 (2012) 1073–1090

Contents lists available at SciVerse ScienceDirect

Gondwana Research

journal homepage: www.elsevier.com/locate/gr

Chemostratigraphic constraints on early Ediacaran carbonate ramp dynamics, Río de la Plata craton, Uruguay

Natalie R. Aubet [a,*], Ernesto Pecoits [a], Andrey Bekker [b], Murray K. Gingras [a], Horst Zwingmann [c,d,e], Gerardo Veroslavsky [f], Héctor de Santa Ana [g], Kurt O. Konhauser [a]

[a] Department of Earth and Atmospheric Sciences, University of Alberta, 1–26 Earth Sciences Building, Edmonton, AB, T6G 2E3, Canada
[b] Department of Geological Sciences, University of Manitoba, 125 Dysart Road (Wallace Building) Winnipeg, MB, Canada, R3T 2N2
[c] CSIRO, Earth Science and Resource Engineering, Bentley W.A., 6102, Australia
[d] School of Earth and Environment, The University of Western Australia, Crawley, W.A. 6009, Australia
[e] Department of Applied Geology, Curtin University, Perth, W.A. 6845, Australia
[f] Instituto de Ciencias Geológicas, Universidad de la República, Iguá 4225, Montevideo, 11400, Uruguay
[g] Gerente Exploración y Producción, ANCAP, Paysandú y Av. Libertador Brig. Gral. J. A. Lavalleja, Montevideo, 11100, Uruguay

ARTICLE INFO

Article history:
Received 7 June 2011
Received in revised form 19 March 2012
Accepted 20 March 2012
Available online 15 April 2012

Handling Editor: I. Safonova

Keywords:
Ediacaran
Basin stratification
Chemostratigraphy
K–Ar illite geochronology
Uruguay

ABSTRACT

C- and Sr-isotope data for marine carbonates can provide a detailed record of isotopic variations in seawater through time and have proven to be a valuable tool for interpreting biogeochemical events and correlating Neoproterozoic sedimentary successions worldwide. Negative carbon isotope excursion to values as low as −4.5‰ in the Ediacaran Polanco Limestones Formation, Uruguay has been interpreted as recording the aftermath of a post-Gaskiers glacial event occurred elsewhere on southwest Gondwana. The record of both deep- and shallow-water settings in the Polanco Limestone Formation provides an opportunity to examine $\delta^{13}C$ variability across the platform and to evaluate whether the carbon isotope values reflect local or global processes. Herein we provide high-resolution $\delta^{13}C$-chemostratigraphy and Sr-isotope data from stratigraphic sections comprising proximal and distal settings on the carbonate platform. Carbon isotopic values are negative in deep-water facies but progressively rise towards positive values in shallow-water settings. This previously unrecognized trend suggests that deposition of Polanco carbonates occurred in a stratified marine basin where degradation of organic matter below the redox boundary led to lower $\delta^{13}C$ values at greater depths. The negative $\delta^{13}C$ excursion is restricted to specific horizons in shallow-water facies and is interpreted as being originated due to higher levels of reworking under storm-dominated conditions, which produced a strong local oxidation of organic matter and ultimately, the negative carbon isotope signatures. $^{87}Sr/^{86}Sr$ and $\delta^{13}C$ chemostratigraphy coupled with new radiometric data allow us to revise the previously proposed age for the unit. This new data support an age between 590 and 560 Ma for the deposition of the Polanco Limestones Formation.

1. Introduction

The geochemical analyses of carbonate rocks has proven extremely useful at unravelling the palaeo-oceanographic conditions during deposition and establishing chemostratigraphic age constraints, particularly when strata lack recognizable fossils or are radiometrically undatable (e.g., Derry et al., 1989; Knoll and Walter, 1992; Jacobsen and Kaufman, 1999; Halverson et al., 2005; Azmy et al., 2006; Bekker et al., 2006; Ohno et al., 2008; Purohit et al., 2010; Sawaki et al., 2010). Based on the premise that carbonate carbon isotope signatures reflect seawater composition at the time of deposition, significant negative carbon isotope anomalies in Neoproterozoic rocks has been interpreted as a proxy of decreased bioproductivity in association with glacial events (e.g., Knoll et al., 1986; Kaufman and Knoll, 1995; Kaufman et al., 1997; Halverson et al., 2005; Zeng et al., 2012). However, secular variations in carbon isotope composition of marine carbonates ($\delta^{13}C_{carb}$) are also known to reflect the influence of several other factors, including post-depositional alteration and diverse sources of the ^{13}C-depleted carbon (Hayes et al., 1999; Knauth and Martin, 2009).

In Uruguay, previous chemostratigraphic studies on Ediacaran carbonates, the Polanco Limestones Formation, have identified a significant $\delta^{13}C$ depletion in shallow-water facies (down to −4.5‰) and a connection to glaciation has been suggested as the most likely explanation for this excursion (Gaucher et al., 2004, 2009). According to the same authors, the absence of glaciogenic rocks associated to this anomaly would be consistent with deposition at low latitudes under tropical conditions and this negative anomaly would reflect seawater composition in the aftermath of a non-global post-Gaskiers glaciation

* Corresponding author. Tel.: +1 780 492 6532; fax: +1 780 492 2030.
E-mail address: aubet@ualberta.ca (N.R. Aubet).

1342-937X/$ – see front matter
doi:10.1016/j.gr.2012.03.011

occurred elsewhere. Crucially, the apparent synchronicity between this excursion, correlated with the Shuram–Wonoka–Johnnie carbon isotope anomaly (Gaucher et al., 2009), and glacial conditions carries important implications for the palaeo-oceanographic and palaeo-climatic evolution in the Ediacaran and ultimately, for the rise of animal life (Canfield et al., 2008; Ishikawa et al., 2008; Maruyama and Santosh, 2008; Meert and Lieberman, 2008; Sawaki et al., 2010; Jiang et al., 2011). In order to assess the extent of this negative excursion across the Polanco basin and therefore, to evaluate the relative contributions of local versus global carbon cycles this study aims to: (a) present detailed carbon isotopic profiles from deep-water and shallow-water facies, (b) constrain the age of the Polanco Limestones Formation by means of new radiometric data, and (c) discuss the possible mechanisms that could have initiated this prominent negative excursion.

2. Geologic setting and stratigraphy

Ediacaran sedimentary and subordinate volcanic rock successions are well exposed on the southeastern and eastern margins of the Río de la Plata craton in Uruguay. These rocks were deposited and deformed during the Neoproterozoic Brasiliano/Pan-African orogeny. This orogeny constitutes the final stages of West Gondwana's assembly (Rapela et al., 2011), which occurred when the eastern margin of the Río de la Plata craton collided along the Sierra Ballena Shear Zone with island-arc terranes that approached from the southeast (Oyhantçabal et al., 2007). The Polanco Limestones Formation forms part of a marine, mixed carbonate-siliciclastic succession, the Arroyo del Soldado Group, which is traceable over 300 km along the eastern border of the Río de la Plata craton and covers an area of approximately 2400 km^2 (Fig. 1). The group reaches almost 3000 m in thickness, and has been subdivided into four formations: the Yerbal, Polanco Limestones, Cerro Espuelitas and Barriga Negra formations (sensu Pecoits et al., 2008; Pecoits, 2010) that record deep- to shallow-water marine environments developed during an overall transgression–regression–transgression (Fig. 2).

At the base, the Arroyo del Soldado Group comprises a fining- and thinning-upward succession with a maximum-recorded thickness of 900 m. It contains interbedded mudstones and sandstones with minor amounts of carbonates, cherts and iron formations (Yerbal Formation). The overlying Polanco Limestones Formation is a coarsening-upward

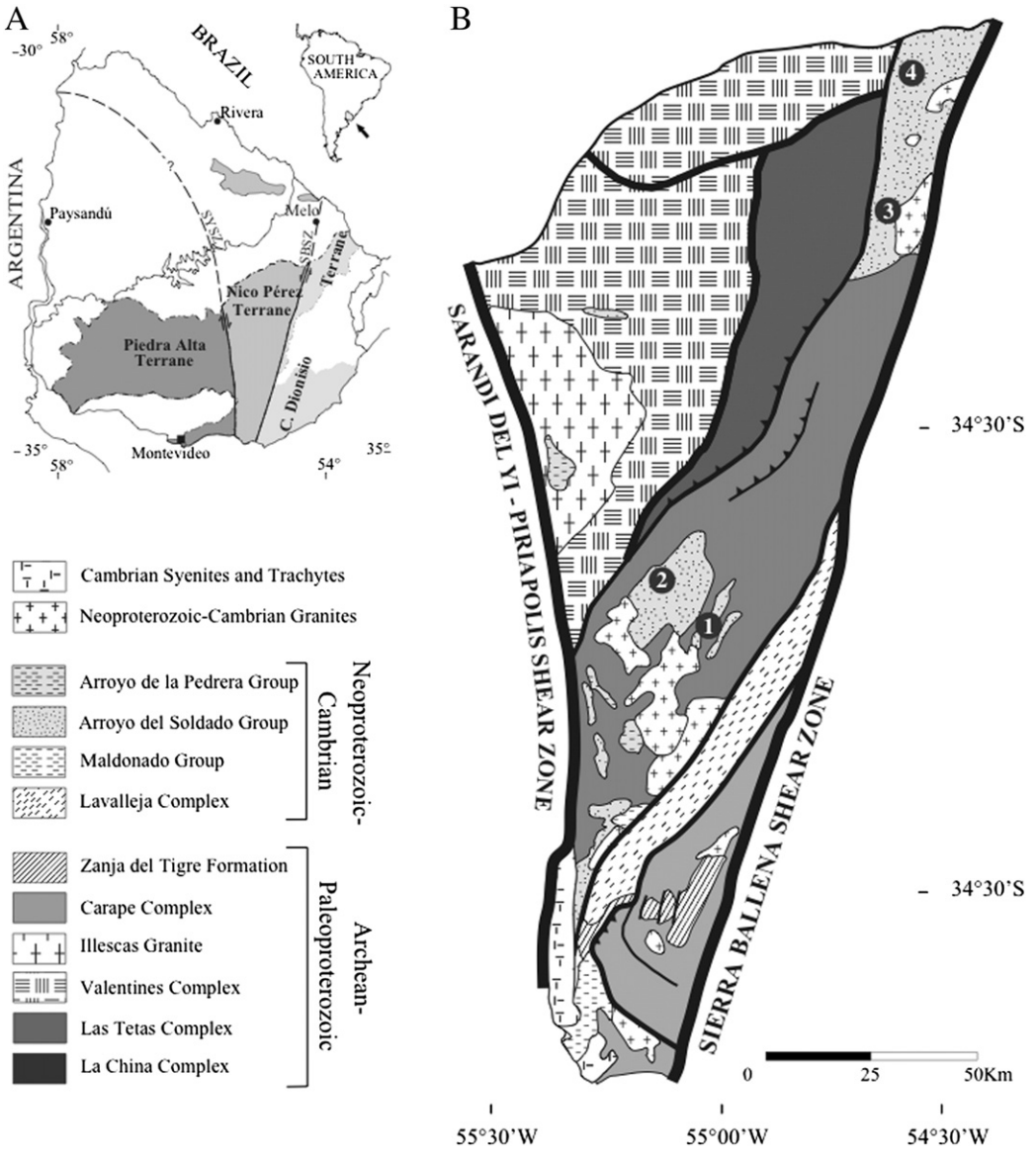

Fig. 1. (A) Location map of Uruguay and tectonostratigraphic subdivision of the crystalline basement (after Bossi, 2003). (B) Schematic geological map of part of the Río de la Plata craton (Nico Pérez terrane; see also Bossi, 2003) showing the distribution of the Arroyo del Soldado Group and location of the sections (1: Los Tapes; 2: Barriga Negra; 3: South Isla Patrulla; 4: Recalde).

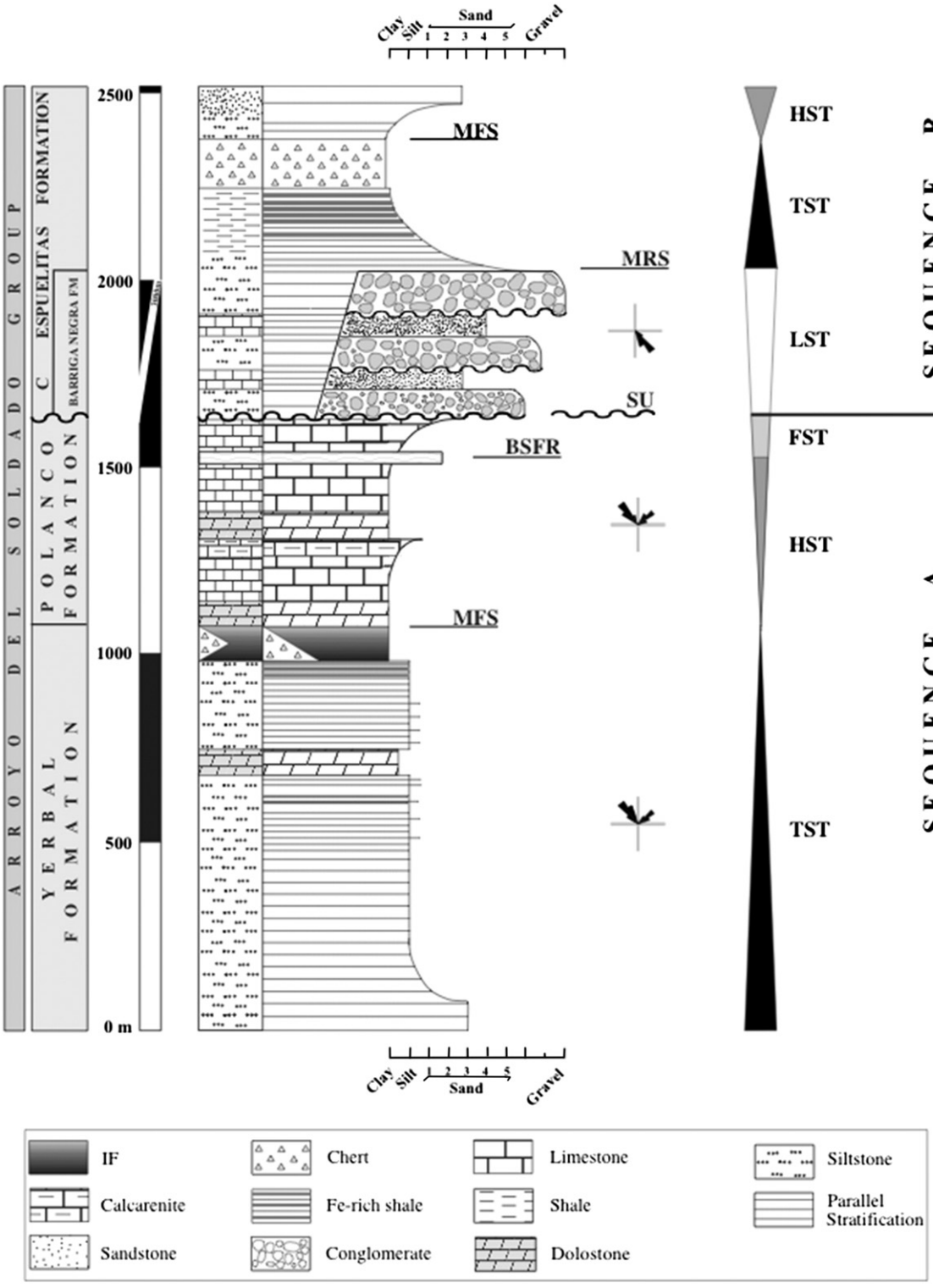

Fig. 2. Simplified stratigraphical column of the Arroyo del Soldado Group (after Pecoits et al., 2008), and sequence stratigraphic interpretation. Abbreviations: SU = subaerial unconformity; BSFR = basal surface of forced regression; MRS = maximum regressive surface; MFS = maximum flooding surface; LST = lowstand systems tract (*sensu* Hunt and Tucker, 1992); TST = transgressive systems tract; HST = highstand system tract; FSST = falling-stage systems tract. Palaeocurrents indicated by rose diagrams.

succession, composed of minor higher-frequency coarsening-upward cycles. Typical lithologies include dark-grey limestones and dolostones rhythmically interbedded on mm- to meter -scales with rare chert layers. Bracketed between siliciclastic units, the carbonate succession thickens from less than 75 m to more than 900 m (Fig. 2). The Barriga Negra Formation is restricted to the western landward margin where it unconformably overlies the Polanco Limestones Formation and consists of basin-margin alluvial fans. The unit comprises thickly bedded conglomerates, carbonate breccias, sandstones and mudstones, which gradationally pass into the Cerro Espuelitas Formation. The latter

consists of an alternation of siltstones, black- and iron-rich shales and cherts, with minor occurrences of sandstones and carbonates and locally reaches a thickness of more than 550 m (Fig. 2).

3. Analytical methods

Rock samples were collected at intervals between 5 and 10 m. Petrographic analyses were performed on sixty-four thin sections, which were stained with Alizarin Red S and potassium ferricyanide to identify calcite, dolomite, and iron content in both mineral phases. Trace element geochemistry was determined using a PerkinElmer Elan6000 Quad-ICP-MS (quadrupole inductively coupled plasma mass-spectrometer) following Na_2O_2 sintering digestion (Longerich et al., 1990). Precision was 4–6% for abundances >0.01 ppm and ≤10% for the most depleted elements.

Carbonate powders were obtained by using a dental drill, and were analyzed for carbon and oxygen isotopes in the Stable Isotope Laboratory at the University of Alberta. Carbonates phases (calcite and dolomite) were extracted separately, and a total of twenty-nine dolostones and fifty-seven limestones were analyzed. CO_2 gas was extracted from these powdered carbonate samples on a high vacuum line by reacting 20–40 mg of sample with 100% phosphoric acid at 25 °C for approximately 24 h of reaction for limestones or 3 days for dolostones (McCrea, 1950). The released CO_2 gas was analyzed for O and C isotopes on a Finnigan MAT 252 mass spectrometer. All carbon-isotope data are expressed in the δ-notation in parts per thousand (‰) using the Vienna Pee Dee Belemnite (V-PDB) international standard. Reproducibility was checked providing an analytical precision of better than ±0.1‰ for $\delta^{13}C$ (1σ) and $\delta^{18}O$ (1σ). From analysis of reference standards, analytical accuracy was estimated to be ±0.1‰.

Strontium isotope ratios of seventeen limestones were determined using 20 mg aliquots of sample powder following the procedures detailed in Holmden et al. (1996). Strontium isotopes were measured using a NuPlasma MC-ICP-MS instrument at the University of Alberta. Subsequent to ion chromatographic treatment, the Sr-bearing aliquots were diluted in a 2% HNO_3 solution and aspirated into the ICP. Strontium isotope data were acquired in static, multicollection mode using five Faraday collectors for a total of 400 s. Prior to the aspiration of a sample, a 30-second measurement of the gas (+acid) blank was conducted for the correction of the ^{86}Kr and ^{84}Kr isobaric (plasma-based) interferences. The isobaric interference of ^{87}Rb was monitored and corrected for using the ^{85}Rb ion signal; however, the latter was negligible for all of the results reported here. Accuracy and reproducibility of the analytical protocol were verified by the repeated analysis of a 100 ppb solution of the NIST SRM 987 Sr isotope standard during the course of this study yielding an average value of 0.710255 ± 0.000020 (1SD; n = 7 analyses) and is indistinguishable compared to the accepted value of 0.710245. The typical internal precision ('error') associated with individual Sr isotope analysis ranges from 0.00001 to 0.00003 (2σ level).

The K–Ar dating was performed on illite samples from the uppermost Yerbal Formation, at CSIRO ESRE facilities, Perth, Western Australia. The sample was gently disaggregated using a repetitive freezing and heating technique to avoid artificial reduction of rock components with K-bearing minerals such as micas or K-feldspars (Liewig et al., 1987). Grain size fractions <2 and 2–6 μm were separated in distilled water according to Stoke's law and a <0.4 μm was separated using a high-speed centrifuge. Clay mineralogy and polytypes were characterized by X-ray Diffraction (XRD). The K–Ar dating technique follows methods described in detail elsewhere (Dalrymple and Lanphere, 1969). Conventional K–Ar isotopic determinations were performed using a VG3600 with an on-line ^{38}Ar spike following Bonhomme et al. (1975). Argon was extracted from the separated mineral fractions by fusing samples within a vacuum line serviced by an on-line ^{38}Ar spike pipette. The isotopic composition of the spiked Ar was measured with an on-line VG3600 mass spectrometer using a Faraday cup. The ^{38}Ar spike was calibrated against biotite GA1550 (McDougall and Roksandic, 1974). During the course of the study 2 standards and 2 airshot values were measured. The K–Ar dating standard and airshot results are summarised in Supplementary Table 1. The error for Argon analyses is below 1% and the $^{40}Ar/^{36}Ar$ value for airshots averaged 294.28 ± 0.29. The K–Ar ages were calculated using ^{40}K abundance and decay constants recommended by Steiger and Jäger (1977). The age uncertainties take into account the errors during sample weighing, $^{38}Ar/^{36}Ar$ and $^{40}Ar/^{38}Ar$ measurements and K analysis. K–Ar age errors are within 2σ uncertainty. See online Supplementary material (Appendix 1) for full details on XRD and radiometric techniques.

4. Results

4.1. Facies associations

Three main facies associations were recognized and interpreted to represent: inner, mid and outer ramp settings (see description below). The scarcity of gravity-induced deposits related to platform margin, the absence of barred restricted marine conditions (e.g., absence of platform-margin buildups), and the gradual transitions between facies suggest deposition on a homoclinal ramp (Read, 1985; Burchette and Wright, 1992).

4.1.1. Medium- to coarse-grained calcarenites with occasional sandstone beds

4.1.1.1. Description. These deposits, up to 200 m thick, are documented in the middle and upper Polanco Limestones Formation at the Recalde and Barriga Negra (parastratotype) sections (see locations in Fig. 1B). Three main facies are recognized in this facies association: (F1) amalgamated hummocky cross-stratified calcarenites (Fig. 3A), (F2) trough cross-stratified calcarenites (Fig. 3B) with sporadic swaley cross-stratification, and (F3) alternations of low-angle cross-stratified and asymmetrically-rippled laminated calcarenites (Fig. 3C and D) showing current direction towards the northwest, although a subordinate, reverse current has also been noted. This facies association typically form coarsening- and thickening-upward regressive units. Facies 1 forms the basal parts of this facies association and overlies mid-ramp deposits (see below) with an erosional contact that locally exhibits rip-up clasts. The dominantly trough cross-stratified calcarenites of F2 commonly appear bracketed between F1 and F3 where the latter, positioned erosionally above F2, occurs at the top of the upper coarsening-and thickening-upward cycles.

4.1.1.2. Interpretation. These deposits are interpreted to represent a storm-dominated inner ramp setting. Facies 1 is taken to represent sedimentation in the upper shoreface environment where well-sorted, low-angle planar cross-bedded calcarenites are interpreted as being produced on a wave-dominated beach face (Dott and Bourgeois, 1982; Dott, 1983). The underlying trough cross-stratified and swaley cross-stratified calcarenites (F2) are characteristic of a storm-dominated middle shoreface environment (Plint, 2011). Trough cross-bedding is generally directed parallel to the shoreline in response to longshore currents; at deeper depths they are sometimes oriented offshore and most likely reflect offshore movement during storms (Hart and Plint, 1989). Thus, the transition from trough cross-stratified and swaley cross-strata into planar cross-stratification and rippled beds with occasional siliciclastic arenite layers suggests a transition to a shallower, higher energy upper shoreface setting where storm and longshore currents were able to form 3-D subaqueous dunes. Hummocky-dominated calcarenites of facies 3 (F3) are interpreted as deposited in the transition between mid-ramp and lower shoreface setting. Their sedimentary structures record frequent storm events indicating water depth above storm-weather wave base (Dott and Bourgeois, 1982).

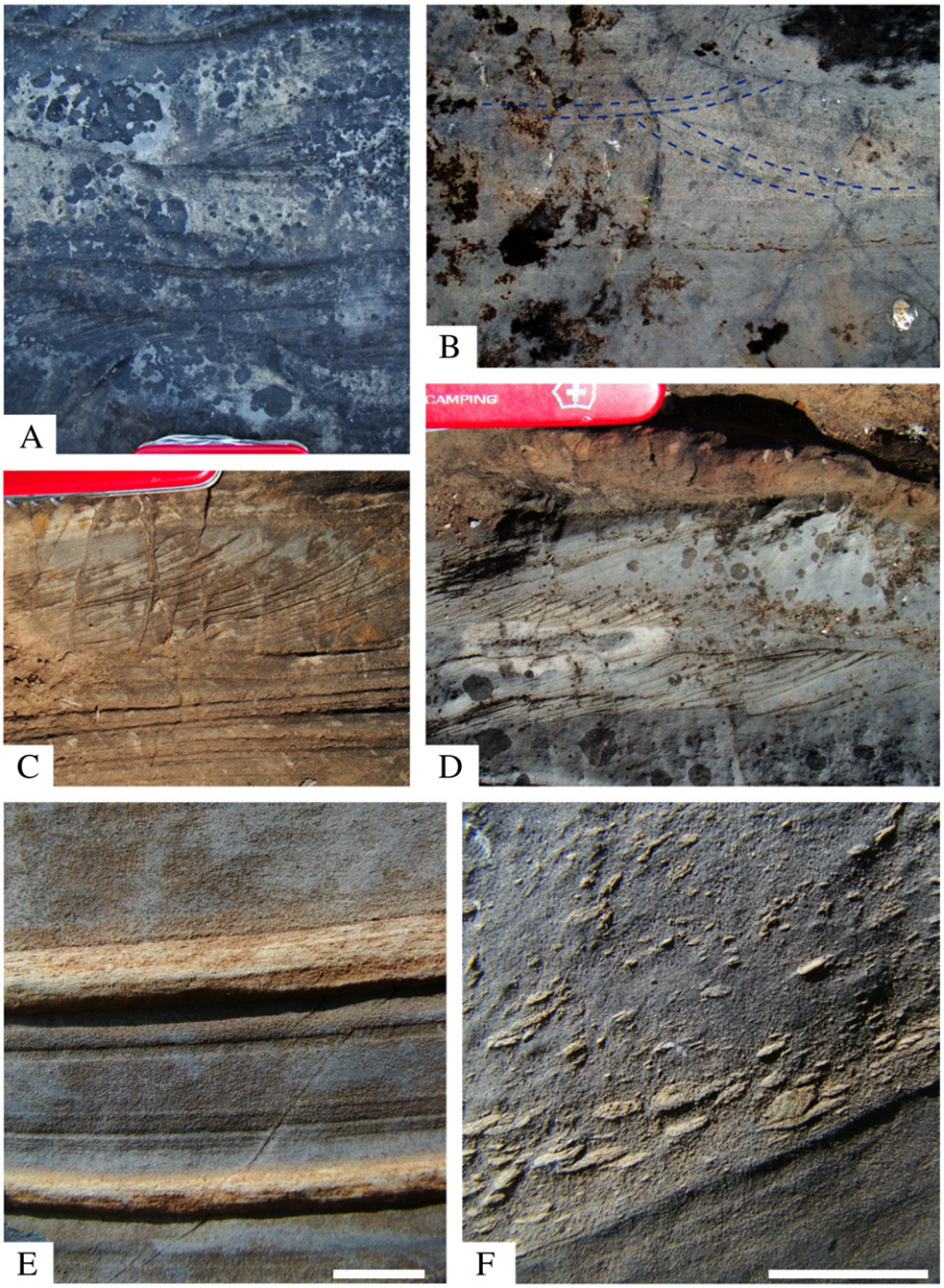

Fig. 3. Inner and middle ramp facies at the Recalde and South Isla Patrulla sections. (A) Hummocky cross-bedded sets in medium grained calcarenites. (B) Trough cross-stratification showing truncation of foreset laminae. (C) and (D) Ripple cross-laminated calcarenites. (E) Grey laminated limestones interbedded with dolostone calcisiltites. (F) Rip-up clasts in normally-graded calcarenite bed. Length of knife = 10 cm; Length of scale bar = 3 cm.

4.1.2. Parallel laminated or thinly interbedded limestone and dolostone calcisiltites

4.1.2.1. Description. This facies association, which is a few meters to more than 200 m thick, is the predominant component within the lower part of the Recalde section and towards the top interfingers with inner ramp facies 3. It is characterized by alternations of grey, parallel laminated or thinly interbedded limestone and dolostone calcisiltites (Fig. 3E). Occasional hummocky cross-stratified calcarenites and thin massive-appearing to parallel stratified calcarenite beds are also present. The finer-grained sediments dominate. Thinner calcisiltite layers are accompanied by correspondingly thinner hummocky cross-stratified beds and calcarenite intercalations. Dark-grey organic-rich, medium to coarse calcisiltites are finely-interbedded with fine dolosiltites layers. Individual layers are a few millimetres to a few decimetres thick, have sharp contacts, tabular geometries and are laterally continuous. The thicker (0.2–2 m) calcarenite beds have erosional bases, particularly when present in association with hummocky cross-stratification, may possess intraformational rip-up clasts at the base and normally graded upper portions (Fig. 3F).

4.1.2.2. Interpretation. The position of this lithofacies in stratigraphic sections and the sedimentary features observed suggest that these finely interbedded carbonates formed in a mid- to proximal outer ramp setting characterized by moderate energy, and episodic storm events as indicated by the hummocky cross-stratification. Likewise, repetitive alternation of fine-grained rhythmites and coarser calcarenite beds reflects alternating storm- and fair-weather deposition in more distal outer ramp areas wherein episodic storms were able to transport coarser sediment into deeper waters (e.g., Seguret et al.,

2001). Thus, hummocky cross-stratified and graded sandstones were formed as storm sheets on the mid-ramp above the storm wave-base, whereas finer sediments were deposited from suspension during periods of quiescence after cessation of storms. Palaeocurrent trends from interbedded coarser lithologies (calcarenites), lateral changes in facies and thickness, as well as the rare slumps measured indicate that the ramp deepened gradually to the southeast and the coastline was roughly oriented northeast-southwest (see palaeocurrent diagrams in Fig. 2).

4.1.3. Laminated to bedded limestones and dolostones

4.1.3.1. Description. These deposits are best represented in the Los Tapes and the south Isla Patrulla sections (see locations in Fig. 1B). Two main facies can be distinguished: (F1) thinly bedded limestone-dolostone (Fig. 4A–D), and (F2) laminated to bedded dolostones. This facies association thickens in the palaeoseaward direction and is characterized by parallel lamination, demarcated by subtle changes in grain size, and occasional chert layers and nodules with no obvious evidence of storm reworking. The limestone and dolostone beds are typically 0.01–1 m thick and grey in color (Fig. 4E). The dolostone layers show well-developed grading and display finer-grain size than the limestone and tend to be thinner and more even-bedded and laminated. Light grey, fine-grained, thin- to medium-bedded dolostones with chert nodules occur at the top of the Polanco Limestones Formation in the distal parts of the basin (e.g., Cerro Espuelitas area).

4.1.3.2. Interpretation. Grain size and sedimentary structures indicate a relatively deep-marine depositional environment characterized by low to moderate energy in an outer ramp setting. The depositional setting was below storm wave base, as suggested by the paucity of graded beds, the presence of fine, parallel lamination and the lack of any evidence of storm or fair-weather wave activity. This facies association was deposited at sufficient depths to be unaffected by wave and storm activity and thus, the cycles recognized in the two other zones are missing in this outer shelf setting. The dark color of the

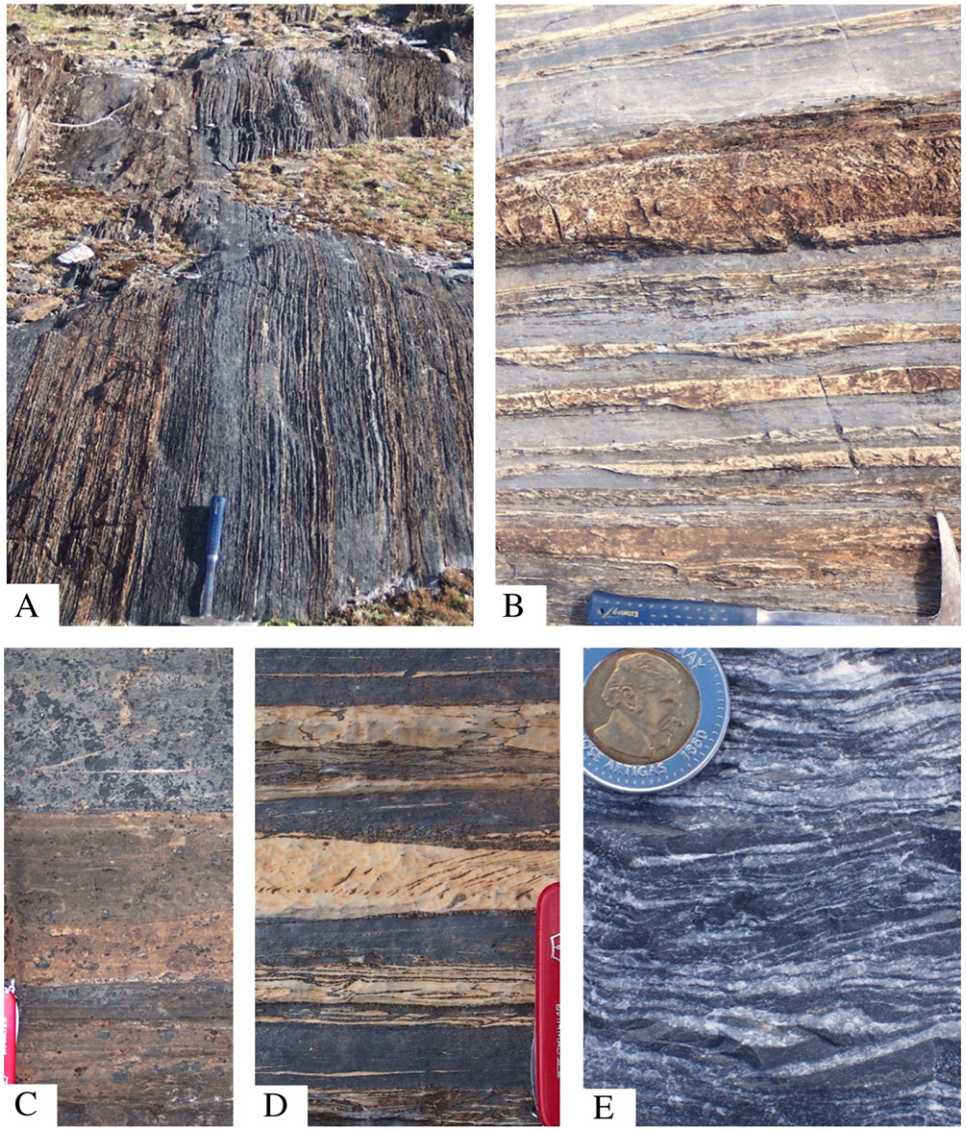

Fig. 4. Outer ramp facies at the Los Tapes section. The carbonate rhythmites represent the most common lithotype of the Polanco Limestone Formation. Rhythmites consist of millimetre- to decimetre-thick alternations of limestone and dolostone layers (A, B). Dolostone predominates over limestone at the base of the section (A). Massive dolostones are usually light beige in color and form beds up to 25 cm thick (C). The contact between dolostone and limestone layers is always sharp, showing no transition (C, D). Color of the limestones is typically gray, with darker colors at the base passing into lighter shades towards the top (E). Weathered dolostone beds commonly have light beige color due to the iron content of the dolomite, while limestone beds weather gray (A, B, C, D). Length of hammer = 40 cm; length of knife = 10 cm.

laminated rhythmites and dolostones, which is due to the organic matter content, suggests anoxic conditions. The poorly-oxygenated, deep-water masses were, however, most likely non-sulfidic as indicated by the abundant organic matter and low S concentrations (<0.012 wt.%) in the dolostones and limestones.

4.2. Petrography

The analysis of the different carbonate phases and microfabric is important to interpret isotopic geochemistry of carbonates. Microscopic observations were conducted in order to identify carbonate components and to evaluate crystal size, percentages of clastic and authigenic minerals, extent of dissolution–recrystallization, and other alteration features. The composition of all studied samples was rather uniform, mostly fine-crystalline dolomite (grain size 5–20 μm) and calcite (<50 μm), with few samples showing partial recrystallization (Fig. 5A–D).

The Polanco carbonates at the Los Tapes and South Isla Patrulla sections are characterized by the alternation of dolostones and limestones (Fig. 4). Two main types of dolostones, massive and laminated, are developed. Massive dolostones are composed of a xenotropic mosaic of subhedral to anhedral fine-grained dolomite crystals (<20 μm) with occasional disseminated euhedral pyrite crystals. Laminated dolostones are composed mainly of an idiotopic mosaic of subeuhedral (planar-s) dolomite crystals with sizes ranging between 5 and 20 μm (Fig. 5A–C). Lamination in dolostones is defined by the presence of variable amounts of silt-sized quartz and authigenic chert (Fig. 5A–B), while the lamination in limestones is composed of fine- to medium-grained equigranular calcite (<50 μm) (Fig. 5C–D). Pressure-dissolution is indicated by micrometer-sized stylolites, which are generally defined by a residue of kerogen or pyrobitumen. Stylolites are common in areas where dolomite and calcite co-occur (Fig. 5A). When present, intercrystalline porosity is occluded by sparry calcite and dolomite cements (Fig. 5D), and, occasionally, chert. Those carbonate cements occur in less than 5% of the rock volume indicating that recrystallization was not extensive. Fractures are usually narrow (up to 25 mm wide) and mineral filled. Two types of fracture-filling cement have been recognized: (1) sub-euhedral blocky spar (>200 μm to <1 cm), and (2) euhedral to sub-euhedral saddle dolomite (>300 μm to <500 μm) (Fig. 5E–F).

The near micritic crystal size and retention of the primary fabric might indicate that diagenesis and deformation did not greatly alter the original sediment. On the other hand, the presence of blocky spar and fracture-healing cements suggest intermediate to deep burial depth for their origin. Therefore, the relative chronology of the diagenetic

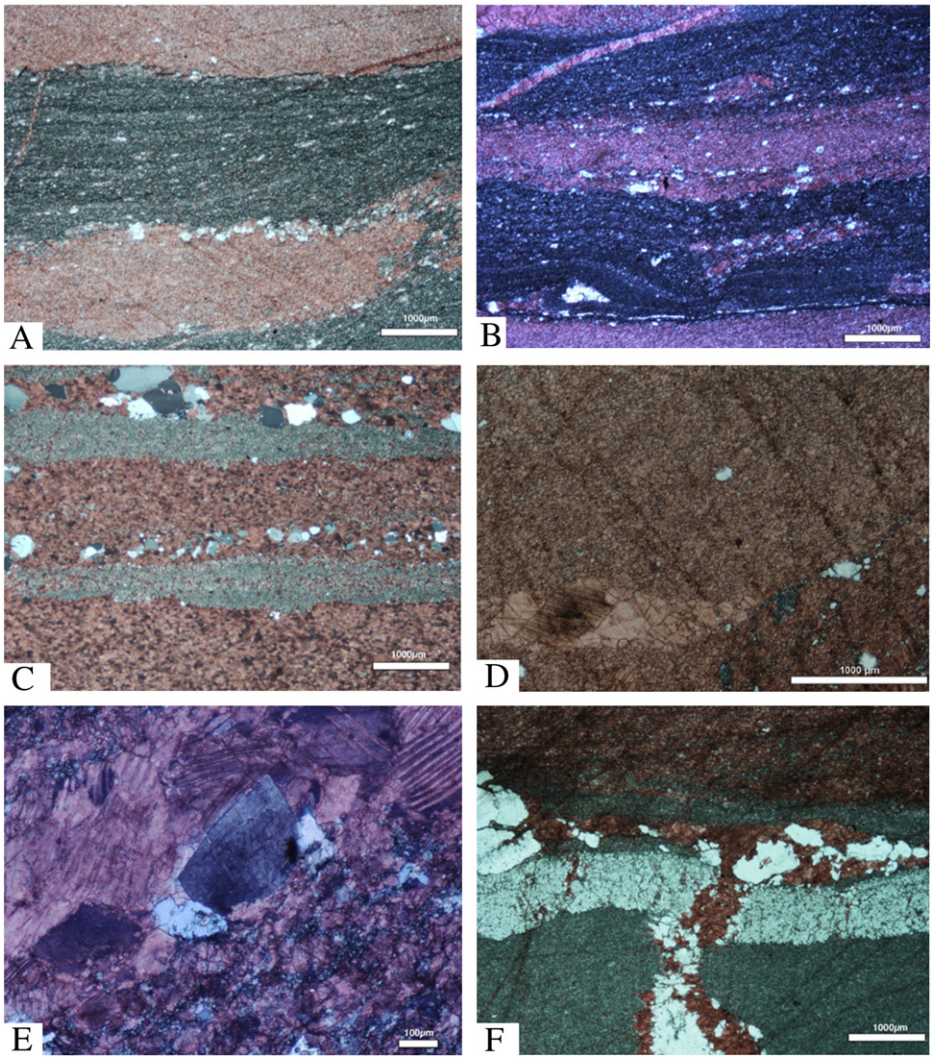

Fig. 5. Thin section microphotographs of carbonate rocks of the Polanco Limestones Formation. Thinly laminated rhythmites show the alternation of microspar laminae with finely laminated dolomicrospar (A, B) and massive impure dolostone laminae (C). Detrital quartz grains are common but never constitute more than the 5% of the rock (A, B, C). Details of fenestral fabric in microspar; blocky calcite occluding porosity (D). Saddle dolomite occurs as a late diagenetic phase filling fractures and in intimate association with subeuhedral blocky spar (E). Silicification pulses were probably contemporaneous with fracturing and carbonate filling (F).

Table 1
Oxygen, C, and Sr isotope values as well as trace element concentrations of carbonates from the Polanco Limestones and Cerro Espuelitas formations.

Unit	Lithology	Sample	$\delta^{18}O_{PDB}$	$\delta^{13}C_{PBD}$	$\delta^{18}O_{SMOW}$	$^{87}Sr/^{86}Sr$	Mn/Sr	Mn	Sr	Al	K	Rb
Polanco Limestone Fm. (Los Tapes)	Limestone	060524/1	−11.969	−0.488	18.572							
Polanco Limestone Fm. (Los Tapes)	Limestone	060524/1	−12.005	−1.65	18.534	0.72436	3.4	216	63.1	5836	8545	14.6
Polanco Limestone Fm. (Los Tapes)	Limestone	060524/2	−10.93	−0.717	19.642							
Polanco Limestone Fm. (Los Tapes)	Limestone	060524/3	−9.25	−1.289	21.374							
Polanco Limestone Fm. (Los Tapes)	Limestone	060524/3	−10.133	−2.246	20.463	0.73083	1.9	148	79.7	4530	5546	9.08
Polanco Limestone Fm. (Los Tapes)	Limestone	060524/4	−13.512	−1.005	16.98							
Polanco Limestone Fm. (Los Tapes)	Limestone	060524/4	−10.288	−2.058	20.304							
Polanco Limestone Fm. (Los Tapes)	Limestone	060524/5	−12.869	−2.273	17.643							
Polanco Limestone Fm. (Los Tapes)	Limestone	060524/5	−9.795	−1.199	20.182							
Polanco Limestone Fm. (Los Tapes)	Limestone	060524/5	-8.86	-1.27	21.776	0.73701	2.4	139	59.0	6933	5240	14.9
Polanco Limestone Fm. (Los Tapes)	Limestone	060524/5	−12.902	−1.287	17.609		2.4	143	58.5	6909	5243	15.0
Polanco Limestone Fm. (Los Tapes)	Limestone	060524/6	−8.393	−1.283	22.258							
Polanco Limestone Fm. (Los Tapes)	Limestone	060524/6	−11.881	−2.146	18.661							
Polanco Limestone Fm. (Los Tapes)	Limestone	060524/7	−13.161	−1.567	17.342	0.73673	1.2	103	84.3	2239	1893	3.35
Polanco Limestone Fm. (Los Tapes)	Limestone	060524/7	−13.161	−1.567	17.342							
Polanco Limestone Fm. (Los Tapes)	Limestone	060524/8	−8.357	−1.815	22.294							
Polanco Limestone Fm. (Los Tapes)	Limestone	060524/8	−11.351	−2.813	19.208							
Polanco Limestone Fm. (Los Tapes)	Limestone	060524/9	−10.872	−1.908	19.702							
Polanco Limestone Fm. (Los Tapes)	Limestone	060524/10	−13.481	−1.697	17.013							
Polanco Limestone Fm. (Los Tapes)	Limestone	060524/11	−10.328	−2.408	20.263	0.73769	2.5	138	55.5	1494	1741	2.42
Polanco Limestone Fm. (Los Tapes)	Limestone	060524/11	−11.977	−3.079	18.563							
Polanco Limestone Fm. (Los Tapes)	Limestone	060524/12	−7.23	−1.622	23.457							
Polanco Limestone Fm. (Los Tapes)	Limestone	060524/12	−7.999	−2.47	22.664	0.74823						
Polanco Limestone Fm. (Los Tapes)	Limestone	060524/13	−13.079	−3.112	17.427							
Polanco Limestone Fm. (Los Tapes)	Limestone	060524/13	−13.676	−2.002	16.811							
Polanco Limestone Fm. (Los Tapes)	Limestone	060524/13	−13.745	−1.973	16.741							
Polanco Limestone Fm. (Los Tapes)	Limestone	060524/14	−8.299	−1.849	22.354							
Polanco Limestone Fm. (Los Tapes)	Limestone	060524/14	−8.622	−2.942	22.022							
Polanco Limestone Fm. (Los Tapes)	Limestone	060524/15	−12.003	−3.179	18.536							
Polanco Limestone Fm. (Los Tapes)	Limestone	060524/15	−9.58	−2.109	21.034							
Polanco Limestone Fm. (Los Tapes)	Limestone	060524/15	−9.58	−2.109	21.034							
Polanco Limestone Fm. (Los Tapes)	Limestone	060524/15	−9.319	−2.165	21.303							
Polanco Limestone Fm. (Los Tapes)	Limestone	060524/15	−11.099	−2.22	19.468							
Polanco Limestone Fm. (Los Tapes)	Limestone	060524/15	−10.105	−2.073	20.493	0.73645	1.6	140	87.0	3238	2682	4.62
Polanco Limestone Fm. (Los Tapes)	Limestone	060524/16				0.74361		256	36.1	15065.8	11735	24.9
Polanco Limestone Fm. (Los Tapes)	Limestone	060524/17	−11.315	−1.53	19.245							
Polanco Limestone Fm. (Los Tapes)	Limestone	060524/17	−12.391	−1.661	18.136							
Cerro Espueltas Formation (Los Tapes)	Limestone	060525/2	−6.405	1.856	24.307	0.74532	10.6	704	66.3	8206	4554	18.6
Cerro Espueltas Formation (Los Tapes)	Limestone	060525/2	−10.227	0.369	20.367							
Cerro Espueltas Formation (Los Tapes)	Limestone	060525/2	−9.999	−1.978	20.602							
Cerro Espueltas Formation (Los Tapes)	Limestone	060525/3	−13.194	−0.944	17.308	0.73100	2.2	249	112	2666	1597	9.60
Polanco Limestone Fm. (Los Tapes)	Dolostone	060524/1	−6.993	0.21	23.701							
Polanco Limestone Fm. (Los Tapes)	Dolostone	060524/3	−7.892	−0.773	22.774		2	161	80.9	4300	5407	8.90
Polanco Limestone Fm. (Los Tapes)	Dolostone	060524/4	−12.312	−0.695	18.217							
Polanco Limestone Fm. (Los Tapes)	Dolostone	060524/5	−12.349	−1.064	18.18		2.3	141	62.5	7476	6141	15.9
Polanco Limestone Fm. (Los Tapes)	Dolostone	060524/6	−10.245	−0.662	20.349		4.9	213	43.6	8204	6871	14.6
Polanco Limestone Fm. (Los Tapes)	Dolostone	060524/8	−7.19	−0.942	23.497							
Polanco Limestone Fm. (Los Tapes)	Dolostone	060524/8	−6.247	−0.915	24.469							
Polanco Limestone Fm. (Los Tapes)	Dolostone	060524/8	−8.59	−1.185	22.055							
Polanco Limestone Fm. (Los Tapes)	Dolostone	060524/9	−11.04	−1.869	19.529		3.2	120	38.1	32448	24590	50.2
Polanco Limestone Fm. (Los Tapes)	Dolostone	060524/11	−10.12	−2.462	20.477							
Polanco Limestone Fm. (Los Tapes)	Dolostone	060524/12	−6.862	−1.591	23.836		6.9	216	31.3	6945	5936	12.6
Polanco Limestone Fm. (Los Tapes)	Dolostone	060524/12	−6.736	−1.613	23.965							
Polanco Limestone Fm. (Los Tapes)	Dolostone	060524/12	−6.674	−1.536	24.03							
Polanco Limestone Fm. (Los Tapes)	Dolostone	060524/13	−9.884	−1.469	20.72							
Polanco Limestone Fm. (Los Tapes)	Dolostone	060524/14	−10.398	−2.715	20.19							
Polanco Limestone Fm. (Los Tapes)	Dolostone	060524/15	−8.411	−1.399	22.239		4.6	249	53.7	6896	5729	8.31
Polanco Limestone Fm. (Los Tapes)	Dolostone	060524/15	−7.246	−1.343	23.44							
Polanco Limestone Fm. (Los Tapes)	Dolostone	060524/15b	−6.638	0.835	24.067							
Polanco Limestone Fm. (Los Tapes)	Dolostone	060524/16	−6.544	−1.776	n		6.2	228	36.6	14049	11199	25.4
Polanco Limestone Fm. (Los Tapes)	Dolostone	060524/17	−11.469	−1.519	19.086		9.6	202	21.1	44653	28517	83.0
Polanco Limestone Fm. (Los Tapes)	Dolostone	060524/17	−12.123	−1.544	18.412		9.7	203	20.9	44647	28892	82.8
Polanco Limestone Fm. (Los Tapes)	Dolostone	060524/17	−11.677	−1.414	18.872							
Polanco Limestone Fm. (Los Tapes)	Dolostone	060524/17	−11.315	−1.53	19.245							
Cerro Espueltas Fm. (Los Tapes)	Dolostone	060525/2	−11.053	−0.489	19.515							
Cerro Espueltas Fm. (Los Tapes)	Dolostone	060525/2	−10.884	−0.247	19.689		12.2	616	50.4	20590	9880	42.9
Cerro Espueltas Fm. (Los Tapes)	Dolostone	060525/2	−11.058	−0.881	19.511							
Cerro Espueltas Fm. (Los Tapes)	Dolostone	060525/2	−10.686	−1.207	19.893							
Cerro Espueltas Fm. (Los Tapes)	Dolostone	060525/2	−10.884	−0.247	19.689		13.2	655	49.6	21392	10246	44.8
Cerro Espueltas Fm. (Los Tapes)	Dolostone	060525/2	−10.704	−0.143	19.875							
Cerro Espueltas Fm. (Los Tapes)	Dolostone	060525/3	−9.534	−0.349	21.082							
Polanco Lmestone Fm (South Isla Patrulla)	Limestone	060526/1	−6.92	−1.65	23.78							
Polanco Lmestone Fm (South Isla Patrulla)	Limestone	060526/2	−8.97	−1.71	21.66							
Polanco Lmestone Fm (South Isla Patrulla)	Limestone	060526/3	−7.89	−1.18	22.77							
Polanco Lmestone Fm (South Isla Patrulla)	Limestone	060526/4	−9.12	−1.23	21.51	0.70710	0.17	91.5	538.24	6113	2875	11.22

Table 1 (*continued*)

Unit	Lithology	Sample	$\delta^{18}O_{PDB}$	$\delta^{13}C_{PBD}$	$\delta^{18}O_{SMOW}$	$^{87}Sr/^{86}Sr$	Mn/Sr	Mn	Sr	Al	K	Rb
Polanco Lmestone Fm (South Isla Patrulla)	Limestone	060526/5	−9.9	−0.56	20.71							
Polanco Lmestone Fm (South Isla Patrulla)	Limestone	060526/6	−8.95	−1.86	21.68							
Polanco Lmestone Fm (South Isla Patrulla)	Limestone	060526/7	−11.34	0.2	19.22							
Polanco Lmestone Fm (South Isla Patrulla)	Limestone	060526/8	−8.65	1.98	22							
Polanco Lmestone Fm (South Isla Patrulla)	Limestone	060526/9	−10.06	0.32	20.54							
Polanco Lmestone Fm (South Isla Patrulla)	Limestone	060526/10	−9.9	0.29	20.71							
Polanco Lmestone Fm (South Isla Patrulla)	Limestone	060526/11	−8.18	0.2	18.24							
Polanco Lmestone Fm (South Isla Patrulla)	Limestone	060526/12	−11.14	0.12	19.42							
Polanco Lmestone Fm (South Isla Patrulla)	Limestone	060526/13	−8.83	1.19	21.81							
Polanco Lmestone Fm (South Isla Patrulla)	Limestone	060526/14	−10.51	1.27	20.07	0.70728	0.12	74.3	619.33	5825	4078	7.2
Polanco Lmestone Fm (South Isla Patrulla)	Limestone	060526/15	−9.33	1.4	21.29							
Polanco Lmestone Fm (South Isla Patrulla)	Limestone	060526/16	−7.87	1.68	22.79							
Polanco Lmestone Fm (South Isla Patrulla)	Limestone	060526/17	−7.906	1.89	22.76							
Polanco Limestone Fm. (Recalde)	Limestone	CDC 1A				0.70791	0.04	37.9	933.3	2213	1732	2.26
Polanco Limestone Fm. (Recalde)	Limestone	CDC 1B					0.25	138.0	544.31	6338	4878	13.7
Polanco Limestone Fm. (Recalde)	Limestone	CDC 1C				0.70722	0.01	36.6	2724.3	1631	2480	3.36
Polanco Limestone Fm. (Recalde)	Limestone	CDC 1F				0.70677	0.06	85.8	1541.9	582	1058	1.00
Polanco Limestone Fm. (Recalde)	Limestone	CDC 2B				0.70723	0.06	125.0	2241.3	2195	3841	10.5
Polanco Limestone Fm. (Recalde)	Limestone	CDC 2B (2)					0.06	126.0	2203.5	2217	3848	10.5
Polanco Limestone Fm. (Recalde)	Limestone	CDC 2D				0.70708	0.13	80.5	626.73	6424	2715	9.39

phases observed in the Polanco Limestones Formation can be summarized as: (1) depositional and immediately post-depositional phases (micritic to microspar dolostones and limestones); and (2) burial phases (blocky cementation of microfenestral cavities, and healing fractures).

4.3. Carbonate geochemistry

4.3.1. Oxygen and carbon isotopes

Results of isotopic analyses on microdrilled carbonates are presented in Table 1 and are plotted relative to their stratigraphic position on Figs. 6 and 7. The range of $\delta^{13}C$ values of dolomite and calcite at the Los Tapes section is narrow (standard deviation for dolomite is 0.8‰ and for calcite is 0.6‰). Carbon isotopic values of dolostones range between −2.7‰ and +0.2‰ (mean = −1.4‰), whereas limestone compositions are between −3.1‰ and −0.4‰ (mean = −1.9‰). The carbon isotope values of both limestones and dolostones show a relatively unimodal distribution, clustered around −1.5‰. At the South Isla Patrulla section (Fig. 7), $\delta^{13}C$ values range between −1.9‰ and +2.0‰ (mean = +0.2‰; standard deviation = 1.3‰). Most of the $\delta^{18}O$ values of the Los Tapes limestones (−7.2 to −13.7‰, mean = −11.0 ± 1.8‰) overlap with the range of the dolostones (−6.2 to −12.3‰; mean = −8.6 ± 2.2‰). The oxygen isotope ratios of limestones in the shallow water facies at Recalde reported by Gaucher et al. (2004) (−6.1 to −10.7‰; mean = −7.9 ± 1.5‰) overlap the field of the deep-water facies limestones of Tapes and those from the South Isla Patrulla section, whereas carbon isotope ratios are more variable in their study (−3.3 to +5.3‰).

4.3.2. Trace elements

Table 1 summarizes the concentrations and ratios of Mn and Sr in the Polanco Limestones Formation at the Los Tapes, South Isla Patrulla and Recalde sections. The dolostones and limestones from Los Tapes have relatively low and constant Mn concentrations ($Mn_{dolostones}$ range between 120 and ± 249 ppm; $Mn_{limestones}$ ranges between 103 and 256 ppm) and Sr contents ($Sr_{dolostones}$ range between 21 and 81 ppm; $Sr_{limestones}$ between 36 and 87 ppm). Sr concentrations are more variable in the Recalde limestones (from 627 to 2241 ppm), corresponding to a narrow range of Mn content (between 37 and 138 ppm). The South Isla Patrulla section shows similar Mn (74–92 ppm) and Sr (538–619 ppm) concentrations as those found in the Recalde section.

4.3.3. Strontium isotopes

The range of Sr isotope values (Table 1) is similar in both South Isla Patrulla ($^{87}Sr/^{86}Sr$ = 0.70710 to 0.70728) and Recalde ($^{87}Sr/^{86}Sr$ = 0.70677 to 0.70791) carbonates. In contrast, Sr isotopic ratios from the Los Tapes section are significantly higher ($^{87}Sr/^{86}Sr$ = 0.72436 to 0.74823).

4.4. Clay mineralogy

The dominant clay minerals present are 2 M_1 illite and kaolinite. The sample fractions contain variable amounts of quartz and 2 M_1 illite is enriched in the finest <0.4 μm fraction (see Supplementary Table 2). No low temperature 1 M/1M_d polytype could be identified by XRD.

4.5. K–Ar dating

Three clay fractions <0.4, <2 and 2–6 μm from sample 101025/1 (uppermost Yerbal Formation) were analyzed. The K–Ar ages are referred to the Gradstein et al. (2004) timescale and vary significantly (Supplementary Table 3). The <0.4 μm illite fraction yields the youngest age of 513.8 ± 10.4 Ma (Cambrian-Series 2-Stage 4). The <2 μm illite fraction yields an intermittent age of 574.7 ± 11.6 Ma (Neoproterozoic–Ediacaran), whereas the coarse grained 2–6 μm illite fraction yields the oldest age of 636.5 ± 12.8 Ma (Neoproterozoic–Cryogenian). Radiogenic ^{40}Ar ranges from 96.4 to 98.9% indicating negligible atmospheric Ar contamination and reliable analytical conditions for all analyses. The K contents range homogenously from 4.2 to 4.3%.

5. Discussion

5.1. Effect of diagenetic alteration on carbonate carbon, oxygen and strontium isotope compositions

A crucial question in any study of carbon isotope composition of ancient carbonates is whether primary marine signature is preserved. One widely-used screening method for evaluating the effects of diagenesis on primary carbon and oxygen isotope compositions is their comparison with absolute and relative trace element abundances (e.g., Brand and Veizer, 1980). For Precambrian carbonates, different abundance ratios and combinations of trace elements and isotopic data are used; one of the most commonly used proxies for post-depositional alteration is the Mn/Sr ratio which is used for assessing post-depositional alterations of $\delta^{13}C$ values (e.g., Kaufman et al., 1991; Jacobsen and Kaufman, 1999; Bekker et al., 2003). During diagenesis, enrichment in Mn is accompanied by the depletion in Sr, increasing the overall Mn/Sr ratios (Brand and Veizer, 1980; Banner and Hanson, 1990). Carbonates with Mn/Sr ratios less than 3.0 are considered to be best-preserved (Derry et al., 1992; Kaufman et al., 1993).

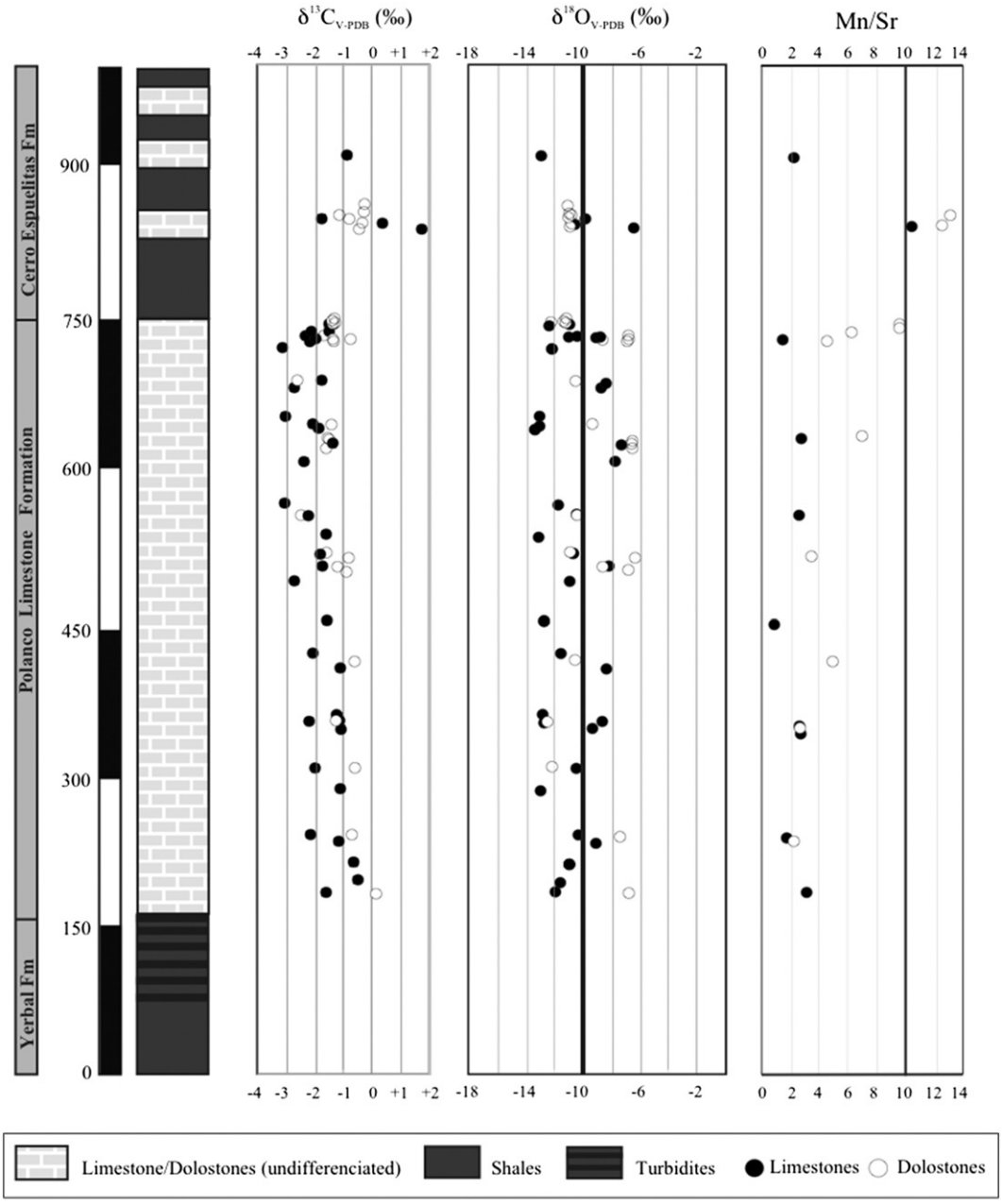

Fig. 6. Schematic stratigraphic profile of the Polanco Limestones Formation at the Los Tapes section and corresponding vertical variations in $\delta^{13}C$, $\delta^{18}O$, and Mn/Sr values.

Strontium concentrations in the Los Tapes section are lower and more homogeneous than those found in the South Isla Patrulla and Recalde areas (see Table 1). The low Sr concentrations in the Los Tapes section, however, do not correlate with an increase in the Mn concentrations, which suggests that both Mn and Sr concentrations are not controlled by the degree of diagenetic alteration. The Mn/Sr ratios of limestones, although lower, are within the range of those displayed by dolostones. This difference might be explained by a better fit of Sr into the crystal lattice of calcite (Veizer, 1983). Although limestones with Mn/Sr ratios above 3.0 might reflect some post-depositional alteration, the consistency of $\delta^{13}C$ values among closely-spaced samples with different Mn/Sr ratios supports a near-to-primary carbon isotope composition. In contrast, Mn/Sr values in the Recalde and South Isla Patrulla areas are <0.25 (Table 1). This difference in Mn/Sr ratios at studied sections may be explained by distinct degrees of alteration in shallow and deep sections. Additionally, the common presence of dolomite in the Los Tapes section (Fig. 5) might be responsible for the overall increase in Mn/Sr ratios of the rhythmites, because Mn easily substitute for Mg during precipitation of either primary or secondary dolomite (Brand and Veizer, 1980; Fairchild et al., 1990; Vasconcelos and McKenzie, 1997). Importantly, the lack of correlation between the Mn/Sr ratios and $\delta^{13}C$ (or $\delta^{18}O$) values and $\delta^{13}C$ values and Mn (or Sr) contents suggests that carbon isotope values from both the Los Tapes and Recalde sections were not strongly influenced by post-depositional alteration (Fig. 8). Therefore, the measured $\delta^{13}C$ values most likely reflect contemporaneous seawater composition.

The $\delta^{18}O$ values can be also used to evaluate diagenetic alteration and the degree of interaction between carbonates and post-depositional fluids (Jacobsen and Kaufman, 1999). As expected, $\delta^{18}O$ values of the dolostones at the Los Tapes section are slightly enriched with respect to coexisting limestones (Fig. 6) (O'Neil and Epstein, 1966). Additionally, the smaller grain size (Fig. 5A and B), earlier stabilization in the post-depositional history and the resulting lower permeability of dolostones might have contributed to better preservation of their original geochemical signature (Pelechaty, 1998). Many of the limestone and dolostone samples display oxygen isotope values above −10‰, similar to

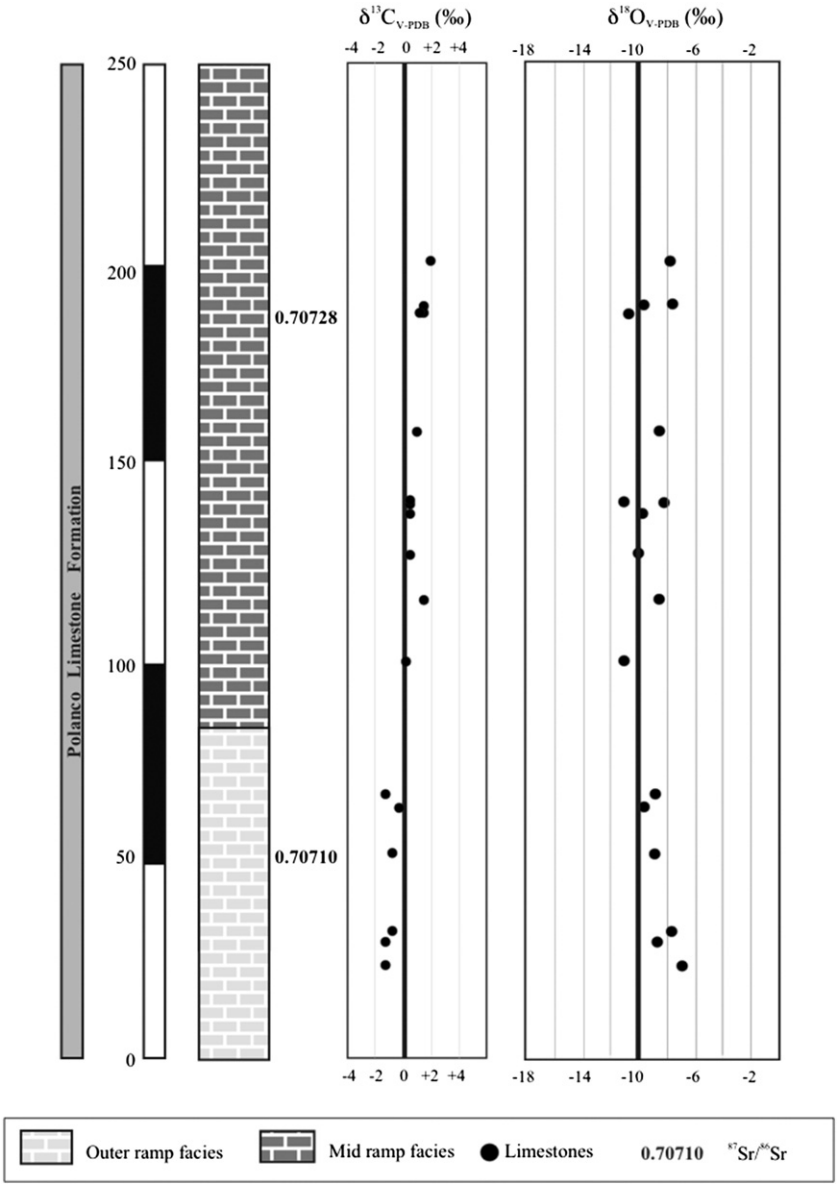

Fig. 7. Schematic stratigraphic profile of the Polanco Limestones Formation at the South Isla Patrulla section and corresponding vertical variations in $\delta^{13}C$ and $\delta^{18}O$ values.

least-altered Neoproterozoic carbonates (Fig. 9) (Kaufman and Knoll, 1995).

Overprinting of primary $^{87}Sr/^{86}Sr$ compositions may result from the mixing of Sr derived from seawater with that derived from external sources (Montañez et al., 1996; Sawaki et al., 2008). Regardless the cause of these elevated values, the $^{87}Sr/^{86}Sr$ ratios from Los Tapes are unlikely to record seawater composition. In turn, the majority of samples from the Recalde area do not show correlation of $^{87}Sr/^{86}Sr$ ratios with $\delta^{13}C$, Mn/Sr or Sr values, which supports preservation of depositional Sr isotope values (Fig. 10).

5.2. C- and Sr-isotope chemostratigraphy

Well-preserved C- and Sr-isotope data obtained for marine carbonates have provided a detailed record of isotopic variations in seawater through time (Melezhik et al., 2001; Shields and Veizer, 2002). Variations in the isotopic composition of carbon in carbonates is a particularly useful indicator of biogeochemical changes over the geological time, reflecting the isotopic composition of carbon inputs to the ocean–atmosphere system, the average fractionation between dissolved inorganic carbon and organic matter, and the proportion of organic matter to carbonate buried in sediments (Kump and Arthur, 1999). In contrast, the $^{87}Sr/^{86}Sr$ of seawater tracks the balance between riverine inputs to the ocean, which result from continental weathering, and inputs from submarine hydrothermal systems (Goldstein and Jacobsen, 1988; Palmer and Edmond, 1989). Hence, $^{87}Sr/^{86}Sr$ ratios are considered a useful proxy to trace global-scale changes in tectonics and climate on a geologic timescale.

The dominant features of the carbon and strontium isotope variations in the Neoproterozoic–Cambrian seawater are generally known, and reference curves of secular variations have been presented by several authors (Melezhik et al., 2001; Halverson et al., 2010a,b; Sawaki et al., 2010; Walter et al., 2000). Characteristic features include: (i) high average $\delta^{13}C$ values ($\approx$5‰) during the Tonian (1,000-850 Ma) and Cryogenian (850–635 Ma), punctuated by three negative $\delta^{13}C$ anomalies during the Bitter Spring Stage and in association with the Sturtian and Marinoan glaciations, (ii) highly variable, and on average low $\delta^{13}C$ values, during the Ediacaran Period, including a distinctive negative anomaly to values as low as −12‰ (Shuram–Wonoka–Johnnie anomaly), and (iii) variable but near average $\approx$0‰ values during the Cambrian, following an apparently short-lived negative excursion at the Precambrian–Cambrian boundary (Halverson et al., 2007; Ishikawa et al., 2008). In contrast, the general pattern of the $^{87}Sr/^{86}Sr$

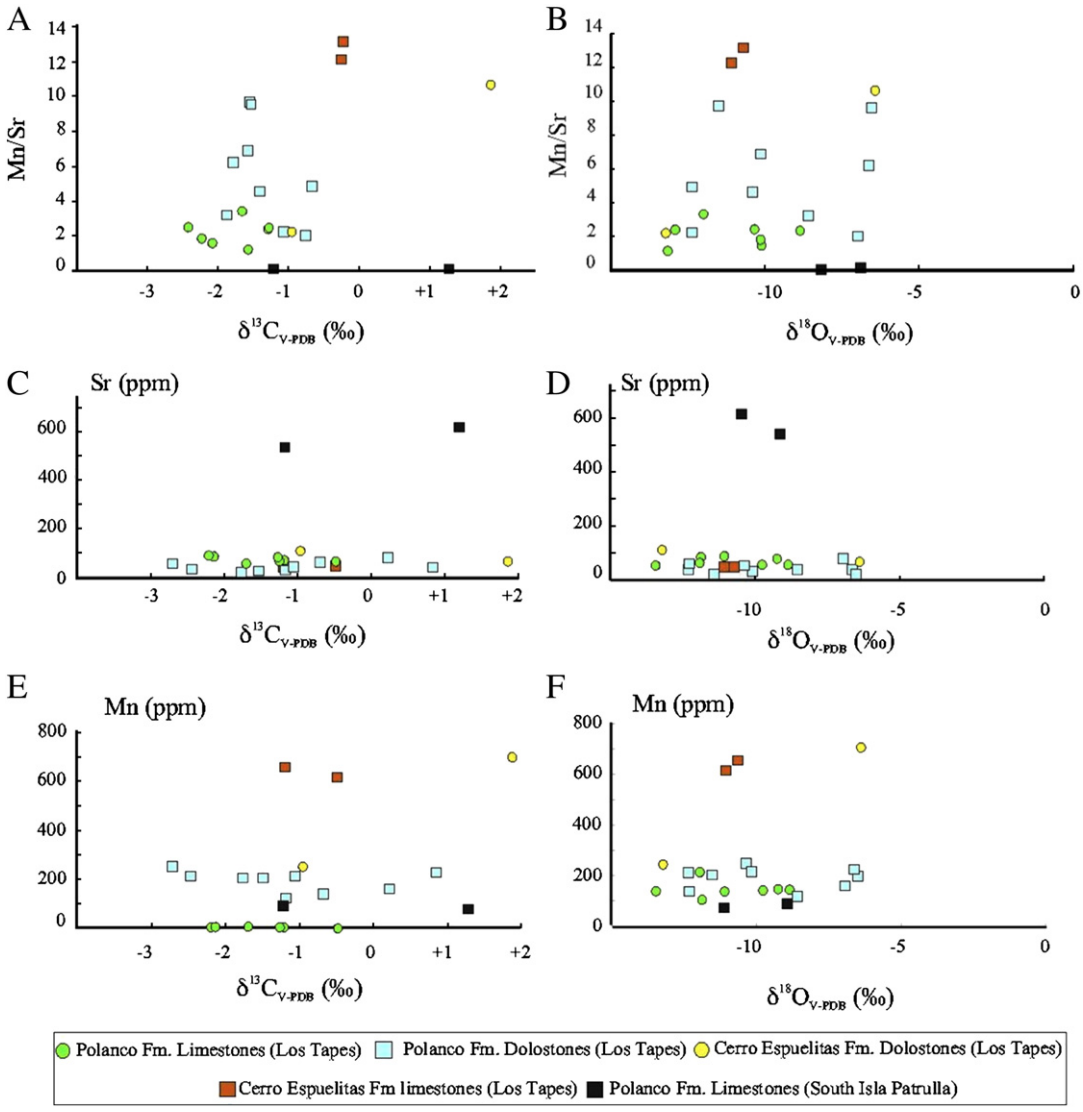

Fig. 8. Scatter diagrams for the Polanco Limestones Formation and the overlying Cerro Espuelitas Formation at the Los Tapes and South Isla Patrulla sections (A) Mn/Sr vs. $\delta^{13}C$, (B) Mn/Sr vs. $\delta^{18}O$, (C) Sr vs. $\delta^{13}C$, (D) Sr vs. $\delta^{18}O$, (E) Mn vs. $\delta^{13}C$, and (F) Mn/Sr vs. $\delta^{18}O$.

record shows a progressive rise through most of the Neoproterozoic (Halverson et al., 2010a,b; Sawaki et al., 2010). However, some differences arise when different compilations are compared. Whereas some authors suggest a virtually monotonic rise with only minor shifts associated with glaciations (e.g., Halverson et al., 2007; 2010b), others have interpreted shifts as discrete, incremental steps (e.g., Melezhik et al., 2001). Overall, low $^{87}Sr/^{86}Sr$ values between 0.7054 and 0.7070 characterize the time span between 900 and 690 Ma, whereas $^{87}Sr/^{86}Sr$ ratios increase from 0.7071 to 0.7086 between 670 and 542 Ma, reaching values as high as 0.7095 in the Cambrian.

As a whole, the carbon isotope composition of the limestones and dolostones of the Polanco Limestones Formation is fairly uniform throughout the Los Tapes section. Other than one exception, all of our values are systematically below 0‰ and the trend shows a gradual shift from +0.2‰, at the base, to −3‰ in the upper part of the section. The South Isla Patrulla section shows a similar trend but with a range of $\delta^{13}C$ values from −1.9‰ to +2‰, and the Recalde section displays more positive $\delta^{13}C$ values ranging from +2.5‰ to +5.3‰ in the lower part of the stratigraphic profile (Fig. 11). These values gradually decrease to −3.3‰, defining a negative excursion, and return to positive values between +0.7‰ and +2.8‰.

The high $^{87}Sr/^{86}Sr$ ratios (>0.72436) of the limestones in the Los Tapes section indicate varying degree of alteration during diagenesis. Limestones with the highest $^{87}Sr/^{86}Sr$ ratios also have much lower Sr contents and thus, were likely more strongly affected by diagenetic fluids. Accordingly, they cannot be used for Sr chemostratigraphy. In addition to the previously reported $^{87}Sr/^{86}Sr$ values (Gaucher et al., 2004; 2009), new $^{87}Sr/^{86}Sr$ data for five limestones from the Recalde (Fig. 11) and two limestones from South Isla Patrulla (Fig. 7) sections were used to chemostratigraphic considerations. The lowest measured $^{87}Sr/^{86}Sr$ ratio (0.70677) is found below the main wave-influenced interval and is from a limestone containing 1541 ppm Sr, which is among the highest concentrations in this study and indicating aragonite precursor, and the lowest content of lithophile elements (Table 1). Furthermore, petrographic observations suggest excellent preservation for this sample, implying that its $\delta^{13}C$ value of +4‰ is probably closest to primary seawater composition.

Following recent compilations of Neoproterozoic seawater Sr isotope curves (Halverson et al., 2010b; Sawaki et al., 2010), most of the samples reported herein (0.70708–0.70791) fall within the range defined for the early Ediacaran (ca. 635–580 Ma). The least radiogenic value obtained (0.70677), however, is significantly lower and would imply either a Cryogenian age (ca. 700 Ma) or, considering a maximum depositional age of 600 Ma for the Polanco Limestones Formation (see $^{40}K-^{40}Ar$ Geochronology below), a contribution from a non-radiogenic source of Sr. The rare earth element plus yttrium pattern for this sample

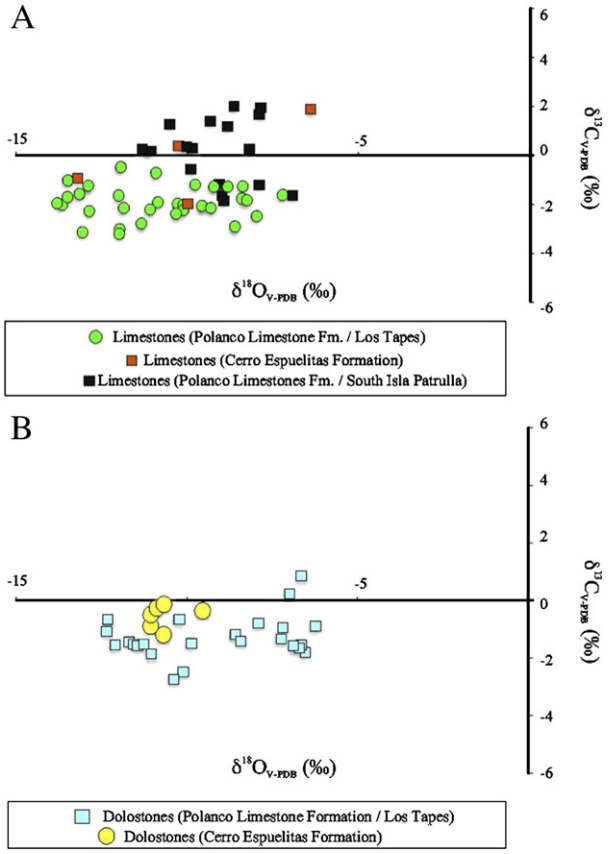

Fig. 9. $\delta^{18}O$ vs. $\delta^{13}C_{carb}$ cross plot for carbonates from the Polanco Limestones Formation and the overlying Cerro Espuelitas Formation at the Los Tapes and South Isla Patrulla sections. The R^2 coefficient of co-variation for the $\delta^{18}O$ and $\delta^{13}C_{carb}$ values for the limestones (A) and dolostones (B) is less than 0.01 indicating no clear correlation between the isotopic data.

share the essential shale-normalized characteristics of marine precipitates (i.e., La, Gd and Y anomalies) but show no Eu anomaly, typical of high-T hydrothermal fluids (see Supplementary Appendix 2) (Bau and Dulski, 1996). In this regard, Pecoits (2010) concluded that iron formations from the uppermost Yerbal Formation were influenced by low-temperature hydrothermal fluids. These young iron deposits differ from typical Archaean and Palaeoproterozoic BIF in that high-temperature hydrothermal input did not influence their chemistry and thus, do not display the characteristic Eu anomaly shown by their older counterparts. Similarly, low-T hydrothermalism could influence the chemistry of the Polanco seawater by lowering its $^{87}Sr/^{86}Sr$ ratio, although not producing positive Eu anomalies.

5.3. $^{40}K-^{40}Ar$ geochronology

According to Gaucher et al. (2004), the maximum depositional age of the Arroyo del Soldado Group is radiometrically constrained by U–Pb crystallization ages of basement rocks from the Puntas del Santa Lucía pluton dated at 633 ± 8 Ma (Hartmann et al., 2002). Minimum age constraints are provided by the intrusive Guazunambí and Polanco granites which yield Rb-Sr isochron ages of 532 ± 11 and 548 ± 11 Ma, respectively (Umpierre and Halpern, 1971; Kawashita et al., 1999). Additionally, the age of the Polanco Limestones Formation is broadly constrained by the youngest detrital zircon U–Pb ages obtained from the underlying Yerbal Formation (~664 Ma) and the overlying Barriga Negra Formation (~566 Ma) (Blanco et al., 2009). This age range is consistent with recently reported K–Ar geochronology of diagenetic illites of the uppermost Yerbal Formation, which indicates a minimum age between 600 and 580 Ma for the unit (Pecoits, 2010). Here, we report new K–Ar illite ages from the uppermost Yerbal Formation to further understand the relative timing of diagenesis in the Yerbal shales and infer the depositional age of the overlying Polanco limestones.

The K–Ar illite ages obtained from the Yerbal shales scatter significantly (from 636.5 ± 12.8 Ma to 513.8 ± 10.4 Ma) but fit within the above mentioned timeframe if considered in the context of a regional very low temperature thermal overprint. Based on the maximum age constraint for the whole group (Puntas del Santa Lucía pluton) and the thermal history of the Arroyo del Soldado Basin, a potential thermal overprint on the ages of the illite fractions was evaluated by basic Ar diffusion calculations as outlined by Zwingmann et al. (2010). Three maximum grain sizes comprising 6, 2 and 0.4 μm and a temperature range of 200 and 250 °C, with a thermal overprint timeframe range of 0.1, 0.5 and 1 Ma, were used. As the geometry of fine grained clay minerals will strongly influence diffusion, cylindrical, plane and sphere geometric shapes were applied. For diffusion calculations of fine grained clay minerals, original parameters listed in Huon et al. (1993) were used in this study with D_o and E_a values 6.03×10^{-7} cm^2/s and 40×10^3 cal/mol respectively (Wijbrans and McDougall, 1986). The results of these calculations are summarized in Supplementary Table 4 and Fig. 12. A potential thermal overprint on the 2 and 2–6 μm grain size fractions is negligible if the temperature is as low as 200 °C up to a modeled 1 Ma range. At a 250 °C range, Argon diffusion will start to reduce the ages of a <0.4 μm fraction whereas the coarser <2 and 2-6 μm fractions will suffer only minor radiogenic ^{40}Ar loss. Calculations indicate that a temperature of 250 °C over a 1 Ma time span would affect and thermally-disturb mainly the ages of <0.4 μm illite fraction. Fig. 12 and Supplementary Table 5 compile recalculated illite ages via a radiogenic ^{40}Ar loss caused by a 0.1, 0.5 and 1 Ma thermal event at 200 and 250 °C on 0.4, 2 and 2–6 μm grain sizes. The average value from cylinder, plate and sphere geometry modeling was used for this calculation. These conditions would suggest indirectly a sedimentation age of the uppermost Yerbal Formation at 600–580 Ma (see Fig. 12).

Therefore, this new data constrain the onset of sedimentation of the Polanco Limestones Formation to a maximum age of 600 Ma. If we assume that the minimum age of deposition is already constrained by the youngest zircons present in the Barriga Negra Formation at ~566 Ma then, the carbonate sedimentation lasted less than 35 Ma. Considering a maximum thickness of ~900 m recorded for the unit, this time frame indicates that the decompacted average sedimentation rate for the Polanco Limestone Formation was ~50 m/Ma. This average value is well within the range of sedimentation rates compiled from similar modern and ancient carbonate systems (Sadler, 1999; Bosscher and Schlager, 1993).

5.4. Palaeo-oceanographic significance of the C- and Sr-isotope records

The long-term secular variations in the carbon isotope composition of marine carbonates ($\delta^{13}C_{carb}$) reflect the influence of several factors. Under steady-state conditions, positive excursions are likely driven by higher productivity due to higher nutrient influx to the surface ocean or an increase in the burial efficiency of organic matter (Halverson et al., 2010a,b). Conversely, negative excursions result from either a decrease in primary productivity or lower burial efficiency of organic matter in sediments (i.e., more organic matter oxidation in the sediments), which ultimately result in decreased burial of organic matter (Halverson et al., 2010a,b). Rapid carbon isotope excursions, especially negative, may also occur under non-steady-state conditions and are most likely a result of input and oxidation of massive amounts of ^{13}C-depleted carbon from sedimentary methane clathrates (Jiang et al., 2003; Bjerrum and Canfield, 2011), labile organic matter (Kaufman et al., 2007), or dissolved organic carbon (Rothman et al., 2003).

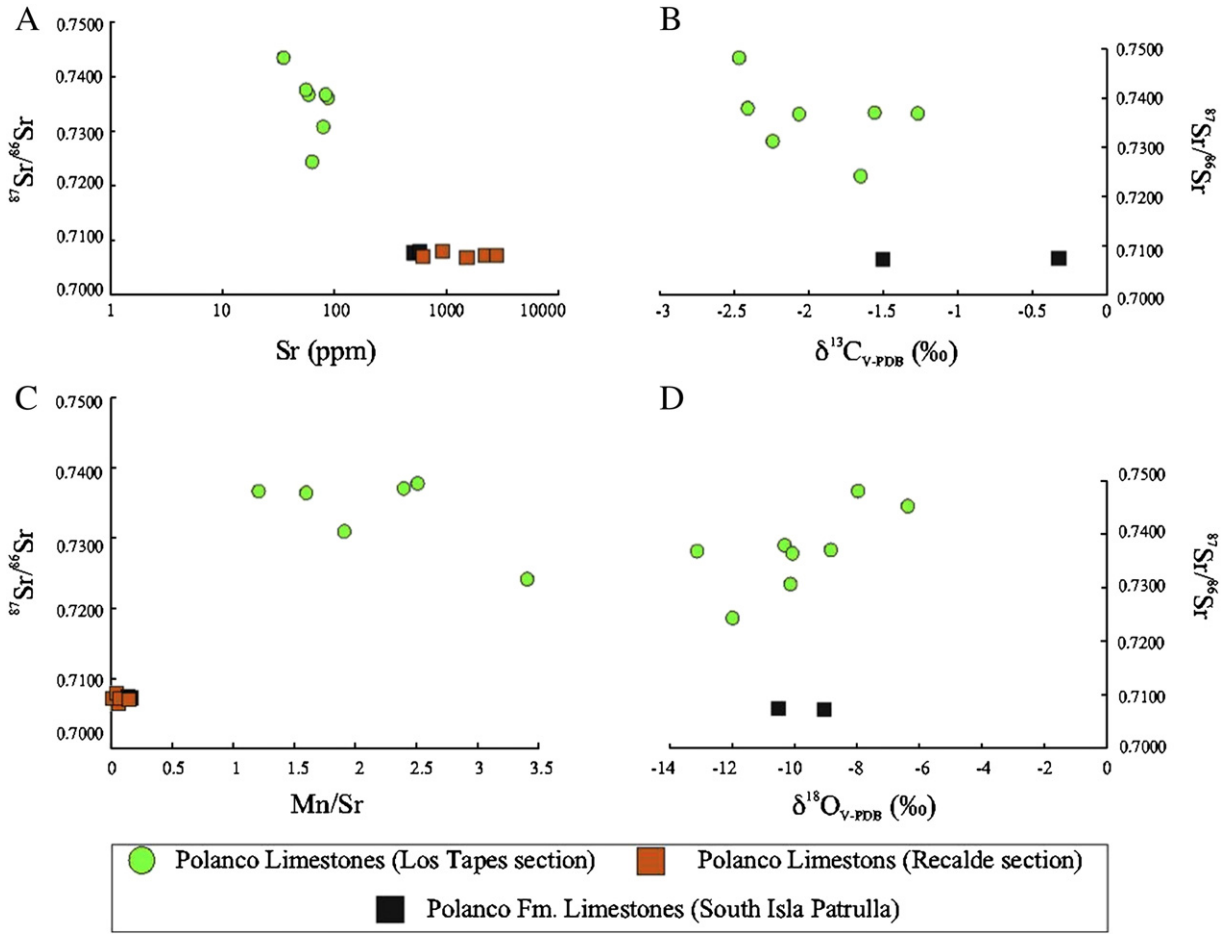

Fig. 10. Scatter diagrams for limestones from the Los Tapes, South Isla Patrulla and Recalde sections. (A) $^{87}Sr/^{86}Sr$ vs. Sr (ppm). $R^2_{Tapes} = 0.15$, (B) $^{87}Sr/^{86}Sr$ vs. $\delta^{13}C$. $R^2_{Tapes} = 0.16$, (C) $^{87}Sr/^{86}Sr$ vs. Mn/Sr. $R^2_{Tapes} = 0.31$, and (D) $^{87}Sr/^{86}Sr$ vs. $\delta^{18}O$. $R^2_{Tapes} = 0.49$.

Comparison of carbon isotope values along a palaeo-depth gradient provides an opportunity to differentiate between local and global signals (Jiang et al., 2007). In this context, critical to the interpretation of the $\delta^{13}C_{carb}$ chemostratigraphy of the Ediacaran Arroyo del Soldado Group and extrabasinal correlations is the understanding of the origin of the $\delta^{13}C$ values recorded by the Polanco Limestones Formation. In the following, we discuss the conditions that might have caused the negative carbon isotope excursion and its palaeo-environmental implications.

5.4.1. Non-steady state conditions

One scenario that could explain the negative carbon isotope values in shallow-water settings is the oxidation of the dissolved organic carbon pool (DOC). The marked ^{13}C-enrichment of Neoproterozoic limestones has been argued to reflect the development of a stratified ocean with a lower anoxic layer depleted in ^{13}C (Kaufman et al., 1991; Derry et al., 1992; Grotzinger et al., 1995; Knoll et al., 1996). These authors hypothesized that intense ocean stratification, with a simultaneous build-up of alkalinity via sulphate reduction and ^{13}C-depletion in anoxic deep waters, might explain the observed geochemical signatures (see also Canfield et al., 2007). This non-steady state process would transfer large volumes of deep-waters with ^{13}C-depleted carbon to the much smaller volume of shallow-water settings, generating large negative $\delta^{13}C_{carb}$ excursions during ocean overturns. Notably some of these large negative $\delta^{13}C_{carb}$ excursions in the Neoproterozoic are not accompanied by parallel $\delta^{13}C_{org}$ excursions, which was explained by a much larger DOC pool in the Neoproterozoic ocean than now (Rothman et al., 2003). It was further suggested that $\delta^{13}C_{carb}$ values would be high at times when the DOC pool was growing (Rothman et al., 2003; Fike et al., 2006; McFadden et al., 2008). The stratified ocean model predicts a ^{13}C-enrichment in carbonates due to high biological productivity in shallow-marine environments and a ^{13}C-depletion in deep waters by remineralisation of organic matter (Knoll et al., 1996; Calver, 2000).

The relative contribution of carbon exchange, between surface and deep ocean waters, to the $\delta^{13}C_{carb}$ signal depends on the water-column structure and depth, as well as on the rates of seawater circulation across the ocean (Calver, 2000). Nonetheless, the Wonoka anomaly can be clearly distinguished from other Neoproterozoic anomalies due to its amplitude ($\delta^{13}C_{carb} < -10‰$) and persistence for several hundred of meters (ca. 700 m) (Le Guerroué et al., 2006; Halverson et al., 2010a,b). Significantly, the carbonates from the Polanco Limestones Formation fall into the range of what are generally considered normal marine carbonates (i.e., $> -5‰$; Summons and Hayes, 1992) and, conversely to the rapid onset of the Wonoka anomaly, the Polanco negative excursion—at the Recalde section—defines a rather gradual trend and persists for no more than 250 m (Fig. 11). Furthermore, a $\delta^{13}C_{carb}$ excursion of the magnitude and duration of the Shuram/Wonoka anomaly, thought to span between 20 and 50 Ma (Le Guerroué, 2010; Wang et al., 2012), should be noticed in different portions of the shelf above the pycnocline. The negative excursion recorded in the Polanco Limestones Formation, however, is facies controlled and only occurs in shallow-water strata associated with storm events and thus, it appears to be likely a local rather than a basin-wide phenomenon.

5.4.2. Steady-state conditions

Negative $\delta^{13}C$ excursions may also indicate an increased rate of oxidation of organic carbon or a decrease in its burial rate (Kump and Arthur, 1999). In this context, the prominent negative excursion

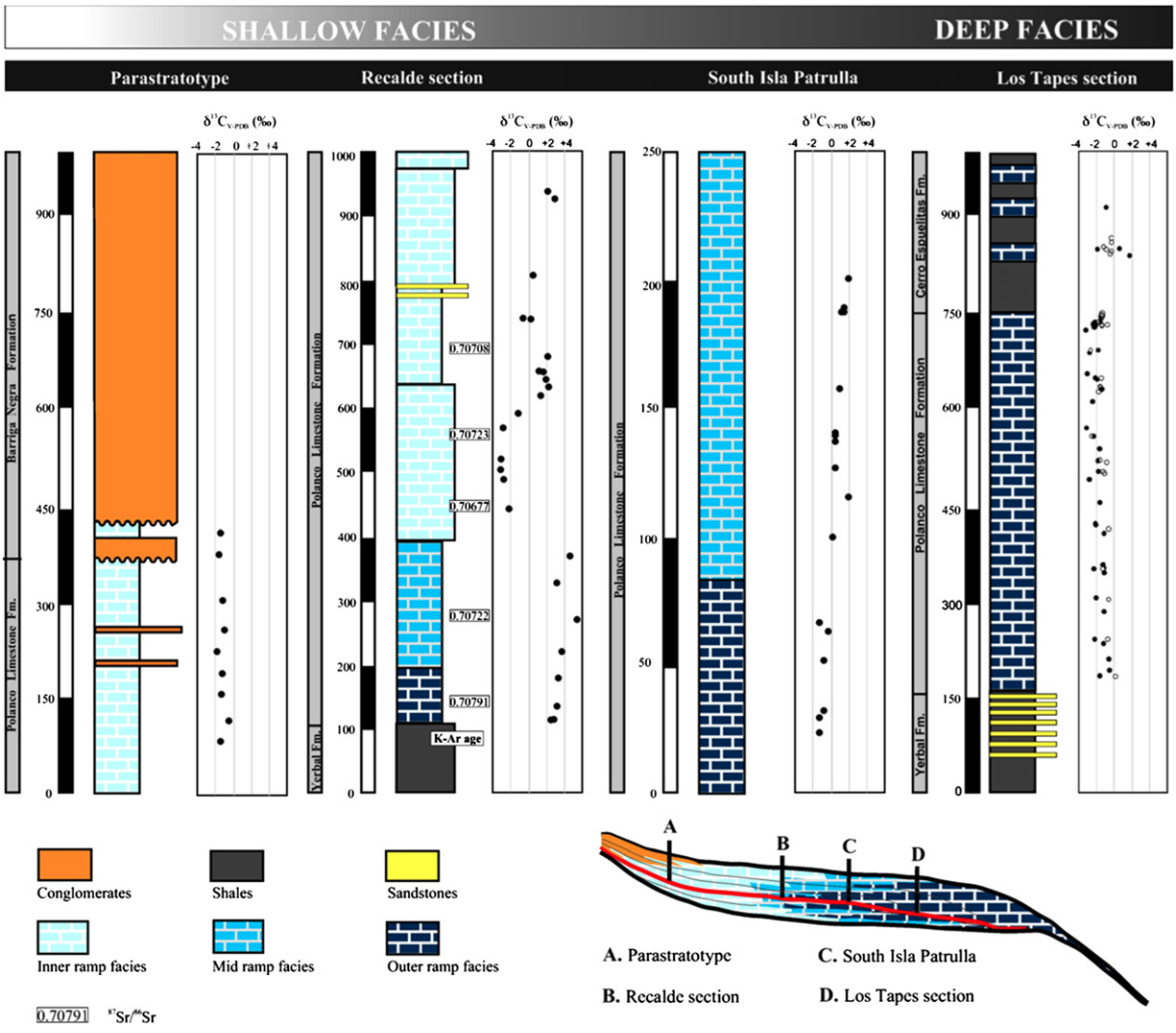

Fig. 11. Comparison of carbon isotope profiles from the deep- and shallow-water sections. Data for the Barriga Negra (parastratotype) and Recalde sections are from Gaucher et al. (2004).

recorded in the middle Polanco Limestones Formation (Recalde section), might reflect recycling of organic carbon either through aerobic respiration in the upper water column (where oxygen was available) or anaerobically in deeper waters or bottom sediment (i.e., sulphate-reducing bacteria). Comparatively, the stratigraphically homogenous and less negative $\delta^{13}C_{carb}$ values ($>-3‰$) found in the more distal Los Tapes section can reflect global carbon isotope signal; i.e., carbon isotope fractionation associated with photosynthetic carbon fixation. In modern oceans, DIC of surface waters is enriched in $\delta^{13}C$ up to 3‰ relative to deeper waters by the 'biological pump effect'; i.e., fixation of carbon in the photic zone and delivery of dead organic matter into deeper waters where it is remineralized (Kroopnick, 1985; Berger and Vincent, 1986). In poorly mixed basins, the difference in $\delta^{13}C_{DIC}$ between surface and bottom waters can be even greater (e.g., 7‰ in the Black Sea; Deuser, 1970). The apparent depth gradient in $\delta^{13}C_{DIC}$ between the shallow- and deeper-water carbonates in the Polanco depositional basin is inferred to have been ca. 2-7‰, which is still comparable to the gradient in modern oceans ($\leq$3‰) and in stratified basins ($\leq$7‰). Water column stratification during the deposition of the lower part of the Arroyo del Soldado Group has been suggested based on the development of iron formation in the upper part of the Yerbal Formation (Pecoits et al., 2008; Pecoits, 2010) and it might explain the difference between the positive and slightly negative carbon isotope values of carbonates in the lower Recalde and Los Tapes sections, respectively. Additionally, when Ce signatures of deep and shallow water facies are compared the former show the absence of Ce anomaly whilst the shallowest samples display negative Ce anomalies (see Supplementary Appendix 2). Such stratification, however, could not have caused the stratigraphically restricted negative excursion found in the tempestitic carbonates of the middle Recalde section; i.e., through oxidation of the DOC pool (see above). In this regard, the carbonate facies of the south Isla Patrulla section, palaeogeographically located between the Los Tapes and the Recalde sections, shows a transition towards consistently positive values best exemplified in the lower Recalde section (Fig. 11). Furthermore, the negative values reached in the shallow tempestite-bearing carbonates are systematically more negative with respect to the ones found in the deeper Los Tapes section providing further support to this hypothesis and arguing against any destratification event.

Hence, the larger carbon isotope gradient between distal (Los Tapes section) and more proximal facies as those recorded in the South Isla Patrulla and lower Recalde sections, could be explained by the effect of a stratified basin. Degradation of organic material below the redox boundary would lead to the mentioned chemical gradient with depth, wherein $\delta^{13}C$ values are more positive in shallow waters. This stratification, however, cannot explain the negative excursion recorded in

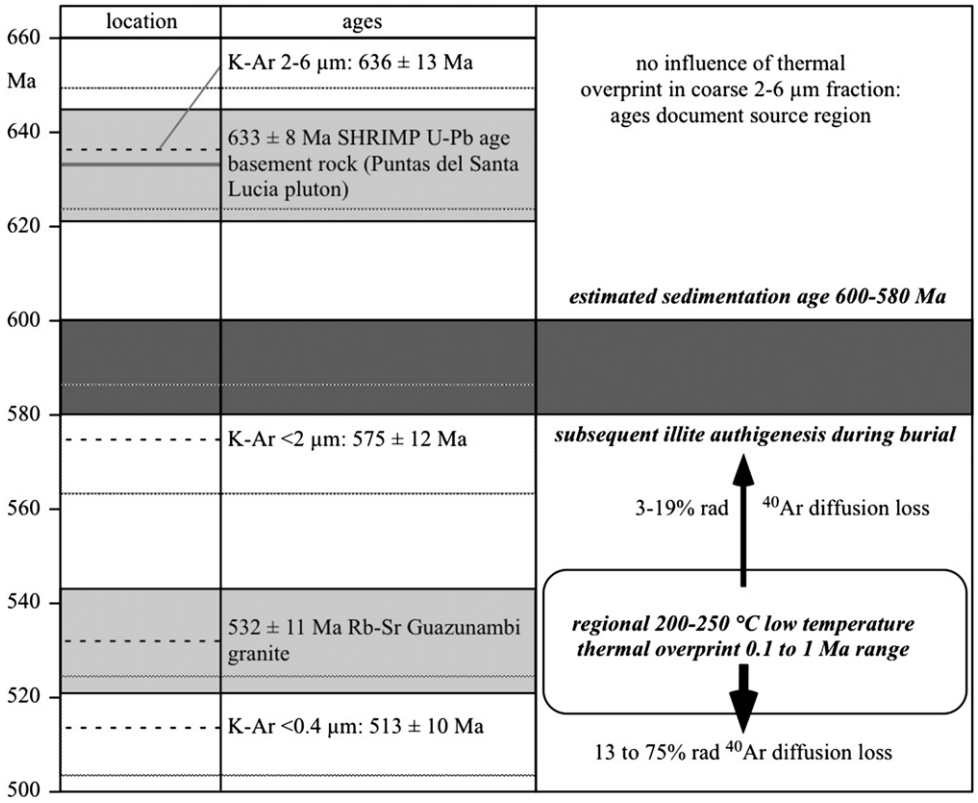

Fig. 12. Summary of the illite age data from the uppermost Yerbal Formation.

storm-related shallow-water facies. According to the view advanced here, the higher levels of reworking under storm-dominated conditions are expected to increase oxidation of organic matter and ultimately, to produce negative $\delta^{13}C$ signatures.

6. Conclusions

Sedimentological, petrographic, geochemical and isotopic data were combined to constrain the depositional environment and the age of the Polanco Limestones Formation and to understand the platform dynamics. By comparing chemostratigraphic profiles across the basin (i.e., shallow- vs. deep-water settings), we show that this type of integrated analysis can help to interpret Precambrian carbonate systems, especially those associated with major palaeo-climatic and palaeo-environmental events. The following conclusions can be drawn from this study:

1. Facies analyses indicate that the Polanco Limestones Formation was deposited on a storm-dominated homoclinal ramp, where inner-, mid- and outer-ramp facies associations were recognized and described. Inner ramp facies association is characterized by coarsening- and thickening-upward regressive cycles of calcarenites representing upper, middle and lower shoreface environments deposited above the mean fair-weather wave base in well-oxygenated waters. Mid-ramp facies association consists of thinly-bedded calcisiltite and dolosiltite with hummocky and swaley cross-stratified calcarenites and thin massive or parallel-stratified calcarenite beds. Outer ramp deposits comprise limestone and dolostone rhythmites and bedded dolostones deposited below the mean storm wave-base and under anoxic conditions.
2. Petrographic observations permits the recognition of two major stages affecting carbonates and their relative chronology: (1) depositional and early diagenetic phases (micritic to microsparitic dolostones and limestones), and (2) late diagenetic phases (blocky and fracture-filling cements).
3. Petrographic, textural and diverse geochemical proxies used here suggest that most of the studied samples did not experience significant post-depositional alteration of the carbon isotope composition and thus, these carbonates record near-primary seawater signature. Accordingly, the carbonates can be used for chemostratigraphic comparisons. In contrast, Sr isotope compositions are more variable, reflecting the effects of diagenesis and probable exchange with clay minerals or simply changes in relative riverine input. In this regard, carbonates from the South Isla Patrulla and Recalde sections are suitable for Sr chemostratigraphy whereas those from the Los Tapes section should be excluded.
4. Carbon and most importantly, strontium isotope data from the Polanco Limestones Formation exhibit values compatible with those of the global seawater reference curves for the early Ediacaran (635–580 Ma). This interpretation is supported by previously reported radiometric data indicating a depositional age between ~600 and ~566 Ma. New radiometric ages on diagenetic illite of the uppermost Yerbal Formation further support this time interval.
5. The lack of a basin-wide negative carbon isotope excursion and good correlation between $\delta^{13}C$ data and facies associations suggests that ramp dynamics strongly influenced the carbon cycle. The results presented are consistent with a strong remineralization of organic matter within the hummocky-bearing inner-ramp sediments, which might account for the most negative $\delta^{13}C$ values in the middle Recalde section. Because organic carbon is ^{13}C-depleted relative to normal marine DIC, precipitation of carbonate derived from remineralized organic carbon will decrease the $\delta^{13}C$ of the limestone and thus, the more efficient respiration of organic matter can produce the negative $\delta^{13}C$ values recorded in these strata. The $\delta^{13}C$ gradient between relatively shallow-water (non-storm dominated) and deep-water facies can be explained by the 'photic pump' effect. When compared with the modern ocean gradient,

the slightly larger $\delta^{13}C$ gradient found in the Polanco Limestones Formation may result from either higher primary productivity at that time, or most likely, a more prominent stratification of the water column.

Supplementary data to this article can be found online at http://dx.doi.org/10.1016/j.gr.2012.03.011.

Acknowledgments

Professor K. Muehlenbachs is gratefully acknowledged for allowing us to use his isotope laboratory facility at the University of Alberta and for his comments on an earlier version of the manuscript. This research was supported by Comisión Sectorial de Investigación Científica (CSIC-Uruguay) and Natural Sciences and Engineering Research Council of Canada (NSERC) Discovery Grants to KOK, MKG and AB. EP acknowledges financial support from the Agouron Institute. NRA acknowledges financial support from the Society of Economic Geologists Student Research Grant and from the Alberta Ingenuity Fund PhD Studentship. A. Todd and M. Raven CSIRO are thanked for technical assistance. Tsuyoshi Komiya and one anonymous reviewer are greatly acknowledged for their thoughtful comments and suggestions to improve the manuscript.

References

Azmy, K., Kaufman, A.J., Misi, A., Oliveira, T.F., 2006. Isotope stratigraphy of the Lapa Formation, São Francisco Basin, Brazil: implications for Late Neoproterozoic glacial events in South America. Precambrian Research 149, 231–248.

Banner, J.L., Hanson, G.N., 1990. Calculation of simultaneous isotopic and trace element variations during water–rock interaction with application to carbonate diagenesis. Geochimica et Cosmochimica Acta 54, 3123–3137.

Bau, M., Dulski, P., 1996. Distribution of yttrium and rare-earth elements in the Penge and Kuruman iron-formations, Transvaal Supergroup, South Africa. Precambrian Research 79, 37–55.

Bekker, A., Sial, A.N., Karhu, J.A., Ferrerira, V.P., Noce, C.M., Kaufman, A.J., Romano, A.W., Pimentel, M.M., 2003. Chemostratigraphy of carbonates from the Minas Supergroup, Quadrilátero Ferrífero (Iron Quadrangle), Brazil: a stratigraphic record of early Proterozoic atmospheric, biogeochemical and climatic change. American Journal of Science 303, 865–904.

Bekker, A., Karhu, J.A., Kaufman, A.J., 2006. Carbon isotope record for the onset of the Lomagundi carbon isotope excursion in the Great Lakes area, North America. Precambrian Research 148, 145–180.

Berger, W.H., Vincent, E., 1986. Deep-sea carbonate: reading the carbon-isotope signal. Geologische Rundschau 75, 249–269.

Bjerrum, C.J., Canfield, D.E., 2011. Towards a quantitative understanding of the late Neoproterozoic carbon cycle. Proceedings of the National Academy of Sciences 108, 5542–5547.

Blanco, G., Rajesh, H.M., Gaucher, C., Germs, G.J.B., Chemale Jr., F., 2009. Provenance of the Arroyo del Soldado Group (Ediacaran to Cambrian, Uruguay): implications for the paleogeographic evolution of southwestern Gondwana. Precambrian Research 171, 57–73.

Bonhomme, M., Thuizat, G.R., Pinault, Y., Clauer, N., Wendling, R., Winkler, R., 1975. Méthode de datation potassium-argon. Appareillage et Technique, Strasbourg, p. 53.

Bosscher, H., Schlager, W., 1993. Accumulation rates of carbonate platforms. Journal of Geology 101, 345–355.

Bossi, J., 2003. Estratigrafía del Precámbrico de Uruguay: terrenos tectono-estratigráficos y geocronología. Revista de la Sociedad Uruguaya de Geología: Rev. Soc. Uruguay. Geol. Spec. Publ., 1, pp. 1–17.

Brand, U., Veizer, J., 1980. Chemical diagenesis of a multi component carbonate system: 1. Trace elements. Journal of Sedimentary Petrology 50, 1219–1236.

Burchette, T.P., Wright, V.P., 1992. Carbonate ramp depositional systems. Sedimentary Geology 79, 3–57.

Calver, C., 2000. Isotope stratigraphy of the Ediacaran (Neoproterozoic III) of the Adelaide rift complex, Australia, and the overprint of water column stratification. Precambrian Research 100, 121–150.

Canfield, D.E., Poulton, S.W., Narbonne, G.M., 2007. Late-Neoproterozoic deep-ocean oxygenation and the rise of animal life. Science 315, 92–95.

Canfield, D.E., Poulton, S.W., Knoll, A.H., Narbonne, G.M., Ross, G., Goldberg, T., Strauss, H., 2008. Ferruginous conditions dominated later Neoproterozoic deep-water chemistry. Science 321, 949–952.

Dalrymple, G.B., Lanphere, M.A., 1969. Potassium–argon dating: principles, techniques and applications to geochronology. W.H. Freeman, San Francisco.

Derry, L.A., Keto, L.S., Jacobsen, S.B., Knoll, A.H., Swett, K., 1989. Strontium isotopic variations in Upper Proterozoic carbonates from Svalbard and East Greenland. Geochimica et Cosmochimica Acta 53, 2331–2339.

Derry, L.A., Kaufman, A.J., Jacobsen, S.B., 1992. Sedimentary cycling and environmental change in the Late Proterozoic: evidence from stable and radiogenic isotopes. Geochimica et Cosmochimica Acta 56, 1317–1329.

Deuser, W.G., 1970. Carbon-13 in Black Sea waters and implications for the origin of hydrogen sulfide. Science 168, 1575–1577.

Dott Jr., R.H., 1983. Episodic sedimentation; how normal is average? How rare is rare? Does it matter? Journal of Sedimentary Research 53, 5–23.

Dott Jr., R.H., Bourgeois, J., 1982. Hummocky stratification: significance of its variable bedding sequences. GSA Bulletin 93, 663–680.

Fairchild, I.J., Marshall, J.D., Bertrand-Sarfati, J., 1990. Stratigraphic shifts in carbon isotopes from Proterozoic stromatolitic carbonates (Mauritania): influences of primary mineralogy and diagenesis. American Journal of Sciences 290, 46–79.

Fike, D.A., Grotzinger, J.P., Pratt, L.M., Summons, R.E., 2006. Oxidation of the Ediacaran ocean. Nature 444, 744–747.

Gaucher, C., Sial, A.N., Blanco, G., Sprechmann, P., 2004. Chemostratigraphy of the lower Arroyo del Soldado Group (Vendian, Uruguay) and paleoclimatic implications. Gondwana Research 7, 715–730.

Gaucher, C., Sial, A.N., Poiré, D., Gómez-Peral, L., Ferreira, V.P., Pimentel, M.M., 2009. Chemostratigraphy. In: Gaucher, C., Sial, A.N., Halverson, G.P., Frimmel, H.E. (Eds.), Neoproterozoic–Cambrian tectonics, global change and evolution: a focus on southwestern Gondwana. : Developments in Precambrian Geology, 16. Elsevier, Amsterdam, pp. 115–122.

Goldstein, S.J., Jacobsen, S.B., 1988. Nd and Sr isotopic systematics of river water suspended material: implications for crustal evolution. Earth and Planetary Science Letters 87, 249–265.

Gradstein, F.J., Ogg, A., Smith, A., 2004. Geologic Time Scale. Cambridge University Press, Cambridge.

Grotzinger, J.P., Bowring, S.A., Saylor, B.Z., Kaufman, A.J., 1995. Biostratigraphic and geochronologic constraints on early animal evolution. Science 270, 598–604.

Halverson, G.P., Hoffman, P.F., Schrag, D.P., Maloof, A.C., Rice, A.H.N., 2005. Toward a Neoproterozoic composite carbon-isotope record. Geological Society of America Bulletin 117, 1181–1207.

Halverson, G.P., Dudas, F.O., Maloof, A.C., Bowring, S.A., 2007. Evolution of the $^{87}Sr/^{86}Sr$ composition of Neoproterozoic seawater. Palaeogeography, Palaeoclimatology, Palaeoecology 256, 103–129.

Halverson, G.P., Hurtgen, M.T., Porter, S.M., Collins, A.C., 2010a. Neoproterozoic–Cambrian biogeochemical evolution. In: Gaucher, C., Sial, A.N., Halverson, G.P., Frimmel, H.E. (Eds.), Neoproterozoic–Cambrian tectonics, global change and evolution: a focus on southwestern Gondwana. : Developments in Precambrian Geology, 16. Elsevier, Amsterdam, pp. 351–356.

Halverson, G.P., Wade, B.P., Hurtgen, M.T., Barovich, K.M., 2010b. Neoproterozoic chemostratigraphy. Precambrian Research 182, 337–350.

Hart, B.S., Plint, A.G., 1989. Gravelly shoreface deposits: a comparison of modern and ancient sequences. Sedimentology 36, 551–557.

Hartmann, L.A., Santos, J.O., Bossi, J., Campal, N., Schipilov, A., Mac Naughton, N.J., 2002. Zircon and titanite U–Pb SHRIMP geochronology of Neoproterozoic felsic magmatism on the eastern border of the Rio de la Plata Craton, Uruguay. Journal of South American Earth Sciences 15, 229–236.

Hayes, J.M., Strauss, H., Kaufman, A.J., 1999. The abundance of ^{13}C in marine organic matter and isotopic fractionation in the global biogeochemical cycle of carbon during the past 800 Ma. Chemical Geology 161, 103–125.

Holmden, C., Creaser, R.A., Muehlenbachs, K., Leslie, S.A., Bergstrom, S.M., 1996. Isotopic and elemental systematics of Sr and Nd in 454 Ma biogenic apatites: implications for paleoseawater studies. Earth and Planetary Science Letters 142, 425–437.

Hunt, D., Tucker, M.E., 1992. Stranded parasequences and the forced regressive wedge systems tract: deposition during base-level fall. Sedimentary Geology 81, 1–9.

Huon, S., Cornee, J.J., Pique, A., Rais, N., Clauer, N., Liewig, N., Zayane, R., 1993. Mise en évidence au Maroc d'événements thermiques d'âge triascico-liasique à l'ouverture de l'Atlantique. Bulletin de la Société Géologique de France 164, 165–176.

Ishikawa, T., Ueno, Y., Komiya, T., Sawaki, Y., Han, J., Shu, D., Li, Y., Maruyama, S., Yoshida, N., 2008. Carbon isotope chemostratigraphy of a Precambrian/Cambrian boundary section in the Three Gorge area, South China: prominent global-scale isotope excursions just before the Cambrian Explosion. Gondwana Research 14, 193–208.

Jacobsen, S.B., Kaufman, A.J., 1999. The Sr, C and O isotopic evolution of Neoproterozoic seawater. Chemical Geology 161, 37–57.

Jiang, G., Kennedy, M.J., Christie-Blick, N., 2003. Stable isotopic evidence for methane seeps in Neoproterozoic postglacial cap carbonates. Nature 426, 822–826.

Jiang, G., Kaufman, A.J., Christie-Blick, N., Zhang, S., Wu, H., 2007. Carbon isotope variability across the Ediacaran Yangtzee platform in South China: implications for a large surface-to-deep ocean gradient. Earth and Planetary Science Letters 261, 303–320.

Jiang, G., Shi, X., Zhang, S., Wang, Y., Xiao, S., 2011. Stratigraphy and paleogeography of the Ediacaran Doushantuo Formation (ca. 635–551 Ma) in South China. Gondwana Research 19, 831–849.

Kaufman, A.J., Knoll, A.H., 1995. Neoproterozoic variations in the carbon isotopic composition of seawater: stratigraphic and biogeochemical implications. Precambrian Research 73, 27–49.

Kaufman, A.J., Hayes, J.M., Knoll, A.H., Germs, G.J.B., 1991. Isotopic compositions of carbonates and organic carbon from upper Proterozoic successions in Namibia: stratigraphic variation and the effects of diagenesis and metamorphism. Precambrian Research 49, 301–327.

Kaufman, A.J., Jacobsen, S.B., Knoll, A.H., 1993. The Vendian record of Sr and C isotopic variations in seawater: implications for tectonics and paleoclimate. Earth and Planetary Science Letters 120, 409–430.

Kaufman, A.J., Knoll, A.H., Narbonne, G.M., 1997. Isotopes, ice ages, and terminal Proterozoic Earth history. Proceedings of the National Academy of Sciences of the United States of America 94, 6600–6605.

Kaufman, A.J., Corsetti, F.A., Varni, M.A., 2007. The effect of rising atmospheric oxygen on carbon and sulfur isotope anomalies in the Neoproterozoic Johnnie Formation, Death Valley, USA. Chemical Geology 237, 47–63.
Kawashita, K., Gaucher, C., Sprechmann, P., Teixeira, W., Victória, R., 1999. Preliminary chemostratigraphic insights on carbonate rocks from Nico Pérez Terrane (Uruguay). Actas II South American Symposium on Isotope Geology, Córdoba, pp. 399–402.
Knauth, L.P., Martin, J.K., 2009. The late Precambrian greening of the Earth. Nature 460, 728–732.
Knoll, A.H., Walter, M.R., 1992. Latest Proterozoic stratigraphy and Earth history. Nature 356, 673–678.
Knoll, A.H., Hayes, J.M., Kaufman, A.J., Swett, K., Lambert, I.B., 1986. Secular variation in carbon isotope ratios from Upper Proterozoic successions of Svalbard and East Greenland. Nature 321, 832–838.
Knoll, A.H., Bambach, R.K., Canfield, D.E., Grotzinger, J.P., 1996. Comparative earth history and late Permian mass extinction. Science 273, 452–457.
Kroopnick, P.M., 1985. The distribution of ^{13}C of $\sum CO_2$ in the world oceans. Deep Sea Research 32, 57–84.
Kump, L.R., Arthur, M.A., 1999. Interpreting carbon-isotope excursions: carbonates and organic matter. Chemical Geology 161, 181–198.
Le Guerroué, E., 2010. Duration and synchroneity of the largest negative carbon isotope excursion on Earth: the Shuram/Wonoka anomaly. Comptes Rendus Geoscience 342, 204–214.
Le Guerroué, E., Allen, P.A., Cozzi, A., Etienne, J.L., Fanning, C., 2006. 50 Myr recovery from the largest negative c excursion in the Ediacaran ocean. Terra Nova 18, 147–153.
Liewig, N., Clauer, N., Sommer, F., 1987. Rb – Sr and K – Ar dating of clay diagenesis in Jurassic sandstone oil reservoirs, North Sea. AAPG Bulletin 71, 1467–1474.
Longerich, H.P., Jenner, G.A., Fryer, B.J., Jackson, S.E., 1990. Inductively coupled plasma-mass spectrometric analysis of geological samples; a critical evaluation based on case studies. Chemical Geology 83, 105–118.
Maruyama, S., Santosh, M., 2008. Models on Snowball Earth and Cambrian explosion: a synopsis. Gondwana Research 14, 22–32.
McCrea, J.M., 1950. On the isotopic chemistry of carbonates and a paleothermometer scale. Journal of Chemical Physics 5, 48–51.
McDougall, I., Roksandic, Z., 1974. Total fusion $^{40}Ar/^{39}Ar$ ages using HIFAR reactor. Journal of the Geological Society of Australia 21, 81–89.
McFadden, K.A., Huang, J., Chu, X., Jiang, G., Kaufman, A.J., Zhou, C., Yuan, X., Xiao, S., 2008. Pulsed oxidation and biological evolution in Ediacaran Doushantuo Formation. Proceedings of the National Academy of Sciences of the United States of America 105, 3197–3202.
Meert, J.G., Lieberman, B.S., 2008. The Neoproterozoic assembly of Gondwana and its relationship to the Ediacaran–Cambrian radiation. Gondwana Research 14, 5–21.
Melezhik, V.A., Gorokhov, I.M., Kuznetsov, A.B., Fallick, A.E., 2001. Chemostratigraphy of Neoproterozoic carbonates: implications for 'blind dating'. Terra Nova 13, 1–11.
Montañez, I.P., Banner, J.L., Osleger, D.A., Borg, L.E., Bosserman, P.J., 1996. Integrated Sr isotope variations and sea-level history of Middle to Upper Cambrian platform carbonates: implications for the evolution of Cambrian seawater $^{87}Sr/^{86}Sr$. Geology 24, 917–920.
Ohno, T., Komiya, T., Ueno, Y., Hirata, T., Maruyama, S., 2008. Determination of $^{88}Sr/^{86}Sr$ mass-dependent isotopic fractionation and radiogenic isotope variation of $^{88}Sr/^{86}Sr$ in the Neoproterozoic Doushantuo Formation. Gondwana Research 14, 126–133.
O'Neil, J.R., Epstein, S., 1966. A method for oxygen isotope analysis of milligram quantities of water and some of its applications. Journal of Geophysical Research 71, 4955–4961.
Oyhantçabal, P., Siegesmund, S., Wemmer, K., Frei, R., Layer, P., 2007. Post-collisional transition from calc-alkaline to alkaline magmatism during transcurrent deformation in the southernmost Dom Feliciano Belt (Braziliano–Pan-African, Uruguay). Lithos 98, 141–159.
Palmer, M.R., Edmond, J.M., 1989. The strontium isotope budget of the modern ocean. Earth and Planetary Science Letters 92, 11–26.
Pecoits, E., Gingras, M., Aubet, N., Konhauser, K., 2008. Ediacaran in Uruguay: palaeoclimatic and palaeobiological implications. Sedimentology 55, 689–719.
Pecoits, E., 2010. Ediacaran iron formations and carbonates of Uruguay: palaeoceanographic, palaeoclimatic and palaeobiologic implications. Unpublished PhD thesis, University of Alberta, p. 230.
Pelechaty, S.M., 1998. Integrated chronostratigraphy of the Vendian system of Siberia: implications for a global stratigraphy. Journal of the Geological Society of London 155, 957–973.
Plint, A.G., 2011. Wave- and storm-dominated shoreline and shallow marine systems, In: Dalrymple, R.W., James, N.P. (Eds.), Facies Models, 4th edition. Geological Association of Canada, pp. 167–200.
Purohit, R., Sanyal, P., Roy, A.B., Bhattacharya, S.K., 2010. ^{13}C enrichment in the Palaeoproterozoic carbonate rocks of the Aravalli Supergroup, northwest India: influence of depositional environment. Gondwana Research 18, 538–546.
Rapela, C.W., Fanning, C.M., Casquet, C., Pankhurst, R.J., Spalletti, L., Poiré, D., Baldo, E.G., 2011. The Rio de la Plata craton and the adjoining Pan-African/brasiliano terranes: their origins and incorporation into south–west Gondwana. Gondwana Research 20, 673–690.
Read, J.F., 1985. Carbonate platform facies models. American Association of Petroleum Geologists Bulletin 69, 1–21.
Rothman, D.H., Hayes, J.M., Summons, R.E., 2003. Dynamics of the Neoproterozoic carbon cycle. Proceedings of the National Academy of Sciences of the United States of America 100, 124–129.
Sadler, P.M., 1999. The influence of hiatuses on sediment accumulation rates. In: Bruns, P., Hass, H.C. (Eds.), On the determination of sediment accumulation rates: GeoResearch Forum, 5. Trans Tech Publications, Switzerland, pp. 15–40.
Sawaki, Y., Ohno, T., Fukushi, Y., Komiya, T., Ishikawa, T., Hirata, T., Maruyama, S., 2008. Sr isotope excursion across the Precambrian–Cambrian boundary in the Three Gorges area, South China. Gondwana Research 14, 134–147.
Sawaki, Y., Ohno, T., Tahata, M., Komiya, T., Hirata, T., Maruyama, S., Windley, B.F., Han, J., Shu, D., Li, Y., 2010. The Ediacaran radiogenic Sr isotope excursion in the Doushantuo Formation in the Three Gorges area, South China. Precambrian Research 176, 46–64.
Seguret, M., Moussine-Pouchkaine, A., Gabaglia, G.R., Bouchette, F., 2001. Storm deposits and storm-related coarse carbonate breccias on a pelagic outer shelf (south–east basin France). Sedimentology 48, 231–254.
Shields, G., Veizer, J., 2002. Precambrian marine carbonate isotope database: version 1.1. Geochemistry, Geophysics, Geosystems 3.
Steiger, R.H., Jäger, E., 1977. Subcommission on geochronology: convention on the use of decay constants in geo-and cosmochronology. Earth and Planetary Science Letters 36, 359–362.
Summons, R.E., Hayes, J.M., 1992. Principles of molecular and isotopic biogeochemistry. In: Schopf, J.W., Klein, C. (Eds.), The Proterozoic Biosphere: A Multidisciplinary Study. Cambridge University Press, Cambridge, UK, pp. 83–93.
Umpierre, M., Halpern, M., 1971. Edades Sr-Rb del Sur de la República Oriental del Uruguay. Revista de la Asociación Geológica Argentina 26, 133–155.
Vasconcelos, C., McKenzie, J.A., 1997. Microbial mediation of modern dolomite precipitation and diagenesis under anoxic conditions (Lagoa Vermelha, Rio de Janeiro, Brazil). Journal of Sedimentary Research 67, 378–390.
Veizer, J., 1983. Chemical diagenesis of carbonates: theory and application of trace element technique. In: Arthur, M.A., Anderson, T.F., Kaplan, I.R., Veizer, J., Land, L.S. (Eds.), Stable Isotopes in Sedimentary Geology: Society of Economic Paleontologists and Mineralogists Short Course No. 10, Dallas (3–1 to 3–100).
Walter, M.R., Veevers, J.J., Calver, C.R., Gorjan, P., Hill, A.C., 2000. Dating the 840–544 Ma Neoproterozoic interval by isotopes of strontium, carbon, and sulfur in seawater, and some interpretative models. Precambrian Research 100, 371–433.
Wang, W., Zhou, C., Yuan, X., Chen, Z., Xiao, S., 2012. A pronounced negative $\delta^{13}C$ excursion in an Ediacaran succession of western Yangtze Platform: a possible equivalent to the Shuram event and its implication for chemostratigraphic correlation in South China. Gondwana Research http://dx.doi.org/10.1016/j.gr.2012.02.017.
Wijbrans, J.R., McDougall, I., 1986. $^{40}Ar/^{39}Ar$ dating of white micas from an alpine high-pressure metamorphic belt on Naxos. Contributions to Mineralogy and Petrology 93, 187–194.
Zeng, J., Cao, C.-Q., Davydov, V.I., Shen, S.-Z., 2012. Carbon isotope chemostratigraphy and implications of paleoclimatic changes during the Cisuralian (Early Permian) in the southern Urals, Russia. Gondwana Research 21, 601–610.
Zwingmann, H., Yamada, K., Tagami, T., 2010. Timing of brittle faulting within the Nojima fault zone, Japan. Chemical Geology 275, 176–185.